Politecnico di Torino

Ingegneria dei Materiali
A.A. 2022/2023
Sessione di Laurea Luglio 2023

3D printing of catalytic reactors for CO_2 transformation

Stampa 3D di reattori catalitici per la trasformazione della CO_2

Relatore:
Dott. Ignazio Roppolo
Co-relatori:
Dott. Victor Sans
Dott.ssa Marcileia Zanatta

Candidato:
Simone Marchetti

Ai miei genitori

TABLE OF CONTENTS

1. INTRODUCTION

The growing global concern regarding climate change and the urgent need for sustainable technologies and practices led to significant research efforts aimed at exploring innovative solutions for carbon dioxide (CO_2) capture and utilization. A key aspect of this effort involves the development of efficient and selective catalytic systems for CO_2 conversion. In this context, additive manufacturing (AM) techniques, such as 3D printing, emerged as promising tools for fabricating catalytic reactors. Consequently, this master's thesis, conducted at the ***Interdepartmental Laboratory*** of **DISAT** (*Dipartimento di Scienze Applicate e Tecnologie*) at "**Politecnico di Torino**" and at the laboratories of **INAM** (*Institute of Advanced Materials*) at "**Universitat Jaume I**" in *Castellon de la Plana, Spain*, initially focused on the creation of 3D-printed catalytic reactors using custom-designed polymer resins optimized to achieve the desired print resolution. Subsequently, the research delved into one specific application, namely, the cycloaddition reaction, whose pathway could offer the opportunity to convert CO_2 into valuable chemicals while reducing environmental impact.

The investigation aimed to address several critical aspects, including the formulation and optimisation of new custom-made photocurable resins suitable for 3D printing of catalytic reactors. These resins were meticulously tailored to achieve the desired print resolution and possess the mechanical properties and chemical stability required for catalytic applications. Furthermore, after functionalising the 3D printed reactors and fully characterising them using a variety of techniques to assess their structural, chemical and thermal properties, we sought to explore their potential for the efficient conversion of CO_2 to cyclic carbonates via the cycloaddition reaction. By using 3D-printed reactors, higher catalytic performance, selectivity and durability were expected.

The aim of this research was to contribute to the advancement of sustainable catalysis and provide insights into the design, optimisation and application of 3D-printed catalytic reactors for CO_2 conversion. The collaboration between the DISAT Interdepartmental Laboratory and the INAM working group facilitated a multidisciplinary approach, combining expertise in materials science, chemistry and additive manufacturing, to address the challenges and explore the potential of 3D printing technology for sustainable catalysis.

1.1 - Additive Manufacturing

Additive Manufacturing (AM) methods, commonly referred to as three-dimensional printing (3DP), have recently expanded rapidly thanks to a range of significant benefits. In details, those are the ability to fabricate intricate geometries with exceptional precision and resolution, unparalleled design flexibility, minimization of waste materials, and the capacity for personalized customization.[1] Furthermore, conventional fabrication methods face constraints in managing the geometry and architecture of macroscopic components maintaining optimal performance, while 3D printing techniques present an efficient approach for engineering precisely controlled functional materials from the nano- to macroscale. AM offers accurate control over geometry parameters such as dimensions, porosity, and morphology, as well as structural characteristics. Furthermore, 3DP pushes the boundaries of materials science and presents a captivating avenue for interdisciplinary research, as it enables the integration of multiple nanomaterials within a single printing process to achieve multifunctional devices.

The origins of 3D printing can be traced back to the 1980s when Charles Hull commercialised the first stereotype process "Stereolithography Apparatus", involving the use of a laser to solidify layers of a liquid resin to build up a three-dimensional object.[2] Throughout the 1990s, other 3D printing techniques emerged and expanded the range of materials that could be used, such as plastics, metals and ceramics; as AM technology improved catering to specific material requirements and enhancing the printing capabilities, it became more accessible and affordable, leading to its widespread adoption across various industries (**Errore. L'origine riferimento**

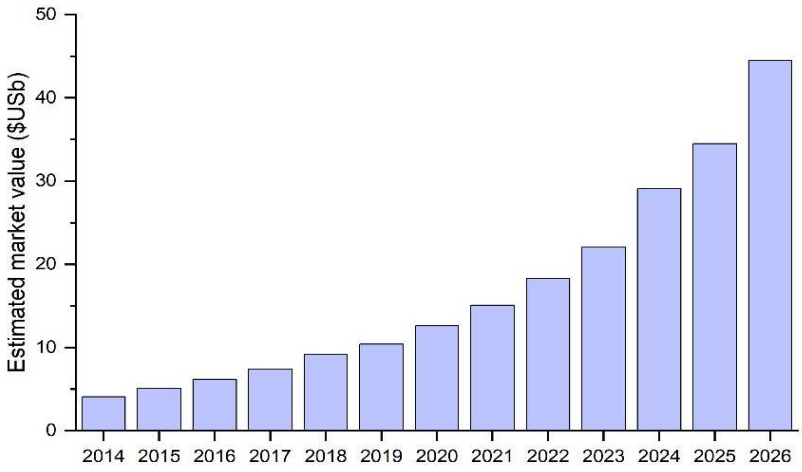

Figure 1 – Graph adapted from 2022 Hubs 3D Printing Trend Report [3]

non è stata trovata.).

Over time, these new techniques were divided by ASTM[1] into seven different classification groups, according to the starting material and to how it is deposited in order to obtain the final object; this classification includes: vat photopolymerization, material jetting, binder jetting, directed energy deposition, powder bed fusion, material extrusion and sheet lamination.[4]

- **Vat Photopolymerization** is a 3D printing technology, that includes Stereolithography (SLA) and Digital Light Processing (DLP), on which this work was based and will be given further explanations later. This printing process is based on the transformation of liquid monomers into macroscopic solids through selective photopolymerization, employing light as energy source. By exposing each layer of the photosensitive formulation to light (usually UV or visible), this undergoes a rapid chemical reaction, which enables fabrication of voxels that, by an iterative process, lead to production of models. Those can be handled and used with limited post-printing process, such as washing and postcuring. Although these additive manufacturing technologies enable the creation of high-resolution objects with intricate details, they are characterized by a relatively slow production speed, significant cost implications, and a limited selection of printable materials.[5]

- **Material Jetting** is based on the deposition of layers of photosensitive polymer resin onto a print platform and on their solidification using UV lights. To ensure consistent layer thickness and remove unnecessary material, a roller is passed over each layer after deposition.[6] Due to the fact that commercial devices have multiple nozzles, this technique offers a broad range of colors and materials, which can let obtain objects using both hard and soft polymers in a single printing process. [1]

- **Binder Jetting** operates similar to Material Jetting. It involves the deposition of a layer of powdered material onto the print bed, followed by the precise application of a liquid binder at selected locations by a print head, thus binding the powder particles together to form the object's layers. This layer-by-layer process continues until the entire object is built. After printing, the excess powder is removed and the object may be subjected to post-processing treatments such as sintering or infiltration to improve its strength and properties. [7]

[1] "ISO/ASTM 52900: 2015 Additive Manufacturing – General Principles – Terminology"[3]

- **Directed Energy Deposition** is widely used for manufacturing high-performance super-alloys. In this technology, a feedstock material is melted through a focused source of energy, like a laser or an electron beam, that in the meanwhile is directed onto a small region of the substrate. The molten material is then deposited and fused onto the substrate, solidifying after the movement of the energy beam. The feedstock is melted before deposition in a layer-by-layer manner with a high energy level required for melting metals. Due to its low accuracy and surface quality and a high speed, it has a limited ability to manufacture complex parts, so it is used for large work envelopes.[1]

- **Powder Bed Fusion** processes consist of thin layers of very fine powders, which are spread and closely packed on a platform. The powders in each layer are fused together with a laser beam or a binder. Subsequent layers of powders are rolled on top of previous layers and fused together until the final 3D part is built. The excess powder is then removed by a vacuum and, if necessary, further processing such as coating, sintering or infiltration are carried out. With this technique, that is characterized by a slow printing speed and high cost, fine resolution and high printing quality can be achieved. This is also due to the fact it does not need the use of support structures because the unfused powder surrounding the printed parts serves as support within the build area. [1] Among these processes there are two that are better known, like Selective Laser Sintering (SLS) and Selective Laser Melting (SLM) [8]: in SLS, the laser scanning process increases the local temperature on the grain surface, leading to fusion/sintering between the powders. SLS can be employed with a wide range of polymers, metals and alloys powders, obviously with different energies according to the material processed. Instead, SLM melts them totally after laser scanning, thus obtaining superior mechanicals properties, but it is limited just to steel and aluminium.[1]

- **Material Extrusion**, in reverse, is a low cost and high-speed technology that uses extrusion of material to fabricate models. Under this umbrella term, two main technologies are acknowledged: fused filament fabrication (FFF) and direct ink writing (DIW). FFF is based on thermal methods and heated extrusion nozzle to heat and soften the material, typically thermoplastic polymer, which is supplied in the form of wire. Once melted, the material is extruded and deposited in layers and then it cools down and solidifies, resulting in the formation of the final geometry.[9] The thermoplastic nature of the polymer filament is necessary in

terms of efficacy of this method, because it enables the filaments to melt together during the printing process and subsequently to solidify at room temperature upon completion. This property facilitates the integration of individual layers, leading to a cohesive and structurally sound final product, even if the layer-by-layer deposition compromises its surface quality.[1] Differently, Direct Ink Writing (DIW) involves the extrusion and deposition of pastes or viscous fluids using mechanical or pressure forces. In this case, it is essential for the paste to possess adequate viscoelastic properties that enable self-sustainability during printing. Alternatively, the paste can be printed within a sacrificial material that provides structural support. Subsequently, the extruded material is typically solidified through various mechanisms, such as thermal, chemical, or light-induced processes.[10]

- **Sheet Lamination** consists in cutting precisely, often thanks to a laser, a thin layer of paper or plastic into the desired shape, which is then pressed by a heated compactor onto the preceding layer. This process activates a special adhesive on the bottom of the sheet making it stick to the substrate. Laminated Object Manufacturing (LOM) employs a type of paper coated on one side with a heat-sensitive adhesive; this paper sourced from a roll is made adhere to the other layers using a heated roller that can activate the adhesive. Since the sheet of material is wider than the actual building area, it has to be cut precisely by a CO_2 laser, that penetrates exactly one layer thickness of the paper, and the edges of the sheet can remain intact to be pulled up by a roll and to keep supplying material for the next layer.[9]

Summarizing, Additive Manufacturing can offer boundless opportunities to create objects with precise shapes and dimensions, thus providing significant advantages to most application fields. Consequently, it led to the exploration of new fabrication methods increasing the number of suitable **applications** in different areas, such as:

Customize Manufacturing - from active electronic materials, electrode and devices to tailored consumer products, Additive Manufacturing enables on-demand production with unique designs and specifications.

Aerospace and Automotive Industries - 3D printing is used to create lightweight, complex parts with intricate geometries, reducing weight and increasing fuel efficiency.

Medical and Healthcare - 3D printing is used to create patient-specific anatomical models for surgical planning, prosthetics, orthotics, and even organ scaffolds for regenerative medicine.

Architecture and Construction - Additive Manufacturing is being explored to create intricate architectural models, scale prototypes, and full-scale buildings, offering the potential for cost-effective, sustainable construction methods and the freedom to design complex structures.[4]

Reactors Design - As it will be shown later in this work, AM techniques have the potential to improve the efficiency of reactors and the field of chemical engineering, primarily due to their extensive customization possibilities; they allow for the creation of reactors specifically designed to accommodate a particular chemistry, rather than adjusting the operational conditions of a standard reactor to suit the desired chemistry.[11] There are examples of 3D-printed reactors that showcase the AM potential in advancing reactor design and performance:

- ***Continuous-flow Reactors*** are designed to facilitate the continuous processing of reactants without the need for batch-wise operations. Their complex and optimized internal geometries enable efficient mixing, enhanced heat transfer, and improved mass transfer. The precise control over channel dimensions, surface roughness, and flow patterns achieved through 3D printing allows for tailored reactor designs to optimize specific reactions. These reactors are particularly advantageous for reactions that require precise control over reaction time, temperature, and reagent ratios. Continuous-flow reactors are widely utilized in various applications, including organic synthesis, pharmaceutical manufacturing, and sustainable chemical processes.[12], [13]
- ***Microfluidic Reactors*** are miniaturized devices that manipulate and control fluids on a micrometer scale (10 – 100μm). Intricate networks of microchannels and chambers are precisely fabricated, enabling the manipulation of small volumes of reagents and facilitating rapid mixing and reaction kinetics. The high surface-to-volume ratio in microfluidic reactors enhances heat and mass transfer, enabling efficient reactions with reduced reagent consumption. These reactors are advantageous for applications requiring precise control over reaction conditions, such as enzymatic reactions, drug screening, and biomedical research.[14]
- ***Catalytic Reactors*** provide increased surface area for catalytic reactions, resulting in improved conversion, selectivity, and reaction rates. These reactors can incorporate catalysts in various forms, including nanoparticles,

coatings, or structured supports, enabling precise control over the catalytic process. 3D printing allows for the fabrication of complex catalyst supports with tailored structures, porosity, and surface properties, optimizing catalyst loading and stability. They find applications in diverse areas, including energy conversion and chemical synthesis.[15]

1.2 - Polymerization process in Vat Photopolymerization

The term "**Vat Photopolymerization**" refers to a specific 3D printing method conducted within a container holding a liquid photopolymer that undergoes selective exposure to UV light. This technology operates on the basis of photopolymerization, a chemical reaction that occurs when light-sensitive liquid inks comprising mono- and multifunctional monomers, photoinitiators, additives, and fillers are polymerized by means of light irradiation. The polymerization starts thanks to the photoinitiator, a chemical compound that is able to absorb the incident light and to generate reactive species (radicals or ions) through the absorption of incident light.[16], [17] The reactive species, upon interacting with the reactive groups present in the monomer, initiate a series of reactions within the resin. Typically, these reactions follow a chain growth mechanism, leading to the formation of polymeric chains (as it is shown in **Figure 2**, adapted from reference [18]). As the reaction progresses, the molecular weight of the system increases, and if the formulation includes cross-linkers, the degree of branching also increases. The type and number of reactive groups present in the monomers/oligomers determine the synthesized macromolecular structures, which can be linear, branched, or cross-linked.[19] The chemical-thermal process involving chain formation is irreversible, and it is not possible to revert prototypes back to their liquid state.[3] Photopolymerization chemistry is extensively utilized in numerous applications, including coatings, adhesives, sealants, printed wiring board resists and microelectronic resists.[20]

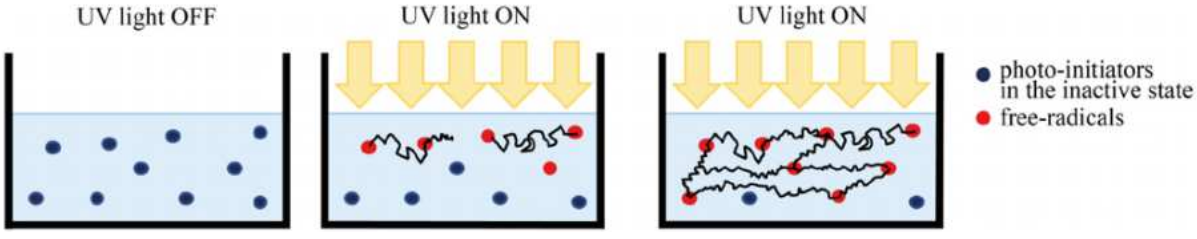

Figure 2 – **Photopolymerization reaction. 1)** The monomer exists in a liquid phase, while the photo-initiators remain inactive. **2)** Upon exposure to UV light, the photo-initiators undergo a transformation, converting into free radicals, **3)** which later engage in reactions with the monomer molecules, facilitating the polymer chains' growth.

During the 3D printing process, the object is constructed layer by layer on a vertically movable platform, with each layer being irradiated by a sufficiently strong light source to initiate the photopolymerization reaction. To ensure the solid parts are insoluble in the liquid resin, a cross-linking polymer is typically added, allowing the material to reach the gel point and obtain a polymeric structure with distinct physical and chemical properties.[21] The advantage of 3D printing lies in its simplicity, as it does not require complex machine configurations or supporting structural materials. The resulting macroscopic models are solid objects that can be utilized immediately. However, a post-printing treatment is commonly employed to remove excess uncured resins. Additionally, photo-curing or heating methods may be utilized to enhance the mechanical properties of the printed object.[22]

Vat polymerization encompasses two distinct fabrication processes: top-down and bottom-up systems (**Figure 3**). In the *top-down system*, the platform descends towards the bottom of the vat, with layers being photopolymerized on the vat's surface. This results in the complete immersion of the printed piece within the photopolymer resin during the build process, while the light source is positioned above the vat. On the other hand, the *bottom-up* configuration involves suspending the printed object above the resin vat. The object is securely held in place on the platform, which moves upward. In this setup, UV light is projected from beneath the optically clear vat window. Currently, the top-down configuration is considered more favourable due to its numerous advantages. It requires less resin since there is no need to cover the entire structure, and it is independent of the bath size. Furthermore, the printable layer remains shielded from the atmosphere, minimizing oxygen inhibition.[23]

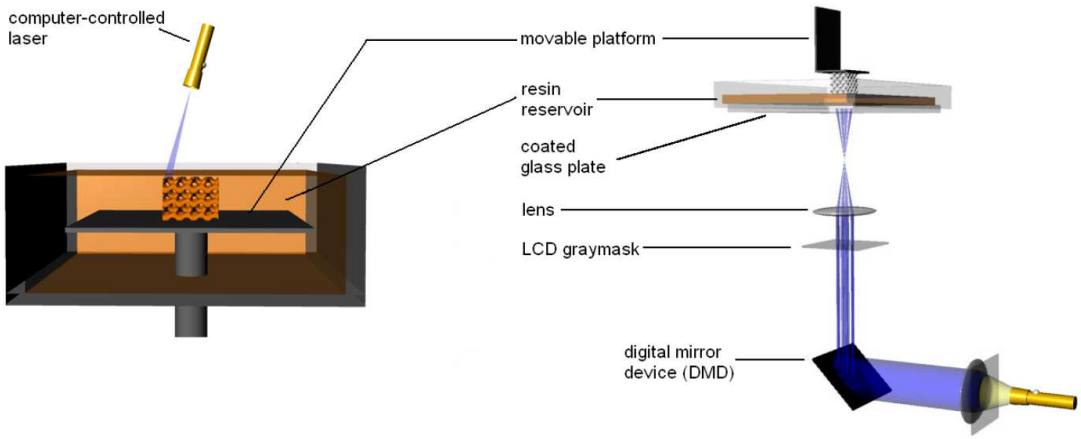

Figure 3 - (***Left***) **Bottom-up** configuration in SLA; (***Right***) **Top-down** system in DLP [23]

- **Stereolithography**, being one of the earliest additive manufacturing (AM) technologies implemented, has firmly established itself in the field. This technique employs a laser beam to draw a customized design on the surface of a photopolymer. Point-by-point, the laser selectively cures the liquid resin present in the vat, operating within the X-Y plane. SLA machines can be configured in either the classical top-down approach, where the platform is positioned below the resin surface, or the bottom-up approach, where the building support is situated above the vat. [23] The top-down methodology, despite its long-standing presence, has drawbacks, such as an extensive cleaning process typically required. As a result, bottom-up systems are gaining increasing prominence. SLA is primarily utilized for the creation of high-quality objects, as it can achieve features smaller than 10 μm with fine resolution. However, it tends to be slower compared to other AM techniques, carries a relatively high cost, and offers a limited range of printable materials. [1] A derivative of SLA technology is *micro-stereolithography* 3D printing (μ-SLA), capable of achieving a minimum feature size of 5 μm. This makes it particularly suitable for the production of very small parts like microcomponents, micromechanisms, and microfabricated devices.[24] *Masked Stereolithography* (MSLA) represents another type of technique where a mask is employed to protect specific areas of each layer during the curing process. This allows for the creation of finer, more detailed layers in the final piece. MSLA is renowned for its exceptional precision and resolution.[25]

- **Digital Light Processing** is a popular 3D printing technique that bears similarities to SLA. Like SLA, DLP employs photopolymerization to solidify liquid resin into solid objects. However, instead of using a laser, DLP printers utilize a digital light projector to selectively expose the resin to light. The projector displays a complete image of each layer, allowing for simultaneous exposure of the entire layer to light. This simultaneous exposure enables faster printing speeds compared to SLA. DLP printers employ a vat of liquid resin and the build platform gradually rises as each layer is cured.[16], [26] In the early stages of this technology, a notable limitation was the substantial quantity of photosetting material required, which also imposed constraints on the height of the printed objects. To address this challenge, an innovative approach was devised, involving the utilization of a transparent adhesive film made from fluorinated ethylene propylene (FEP) as the bottom of the vat. This modification proved instrumental in DLP 3D printers, as it minimized the amount of photosensitive material necessary for each printing operation and surpassed the height limitations by allowing the printed object to be "pulled out" from the liquid resin bath. Consequently, this advancement enabled more efficient and flexible printing processes, enhancing the capabilities of DLP technology in terms of material usage and the size of the printed

objects.[27] The printed object undergoes cleaning and post-processing to attain the desired properties. DLP is renowned for its speed and capacity to produce smooth and intricate prints, making it suitable for applications such as rapid prototyping, customized manufacturing, and the production of dental items. In DLP maximum resolution depends primarily on the dimension of pixels, which follow the dimensions of the micromirror of the DMD (Digital Micromirror Device), which is the core of this equipment and also determines its price. Considering the equipment actually available on the market, the minimum resolution is around 20x20 μm^2, but this depends also on other factors such as printing parameters and resin reactivity. [16], [26]

Both SLA and DLP technologies offer distinctive advantages and have made significant contributions to the advancement of 3D printing. They provide precise and detailed prints with excellent surface finish, facilitating the creation of intricate designs and functional prototypes. As 3D printing continues to evolve, these techniques, along with other innovative methods, will play an increasingly pivotal role in transforming industries and shaping the future of manufacturing.[28]

Each 3D printing method necessitates the preparation of a tailored set of specific instructions to the 3D printer. While all these instructions vary according to the printer type and printing technique employed, they all share a common element: the 3D model, that is generated using *computer-aided-design* **(CAD)** *software* and is translated into a format understood by the printer that is named **STL file** format (short for stereolithography). Within STL format files, the geometry of the 3D object is stored as a mesh comprising interconnected polygons representing its surfaces. To communicate effectively with the 3D printer, a series of commands must be prepared based on the geometry extracted from the STL file and a specialized slicer software has been developed to achieve this: the primary function of slicers is to divide the original 3D model into a sequence of cross-sections based on operator-defined parameters. An example of how STL files look like and how slicer software works is shown in **Figure 4.**

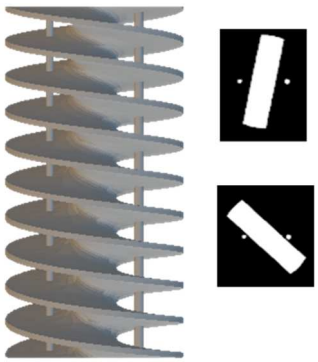

Figure 4 – (***Left)*** STL image of a catalyser; (***Right***) Sliced cross-section of the same catalyser.

For technologies employing laser heads or printheads, the cross-sections of the model need to be further subdivided into paths that the printhead will traverse. In methods where the printing process relies on following these paths, the spatial resolution significantly depends on the slicer software's settings, such as path width and height. Path width determines the horizontal (x-y plane) resolution, while path height influences the vertical (along the z-axis) resolution. Reducing the values of path height and width improves the shape accuracy of the printed elements but at the expense of increased printing time. The output file resulting from the slicing operation contains a collection of commands, comprehensible to the printer driver, saved in the **gcode text file format*. Once these commands have been set, the printer is capable of reproducing a geometric object using the appropriate material. However, the actual spatial resolution of the resulting 3D printout may vary due to factors such as the device's design and the quality of the machine code implemented.[27]

1.3 - Photocurable resins for 3D printing

As detailed above, photocurable formulations, as the liquid precursors of polymeric materials, can undergo polymerization through light irradiation. Photopolymerization offers rapid polymerization rates, even at room temperature, requires low energy input, allows for the use of solvent-free formulations, and according to the photoinitiator characteristics, enables a broad range of wavelengths to initiate the process. Furthermore, it offers spatial-temporal control as the polymerization can be precisely tuned by adjusting the light settings. One of the key advantages of light induced 3D print is its inherent flexibility, allowing the resins to be customized and tailored to meet specific requirements by adding proper ingredients. This feature enables the development of materials with desired properties and functionalities, making this technology highly suitable for a wide range of applications.[1] The integration of constituent elements including monomers, active materials, photoinitiators, and additives needs a meticulous optimization to attain the desired resolution along with tailored properties encompassing chemical, mechanical, optical, and other relevant characteristics. [29]

Typically, the composition of photocurable formulation for 3D printing includes a combination of various components:

- ***Monomers and oligomers*** are compounds (usually liquid but can be also solid but soluble) that contain reactive groups essential for the formation of a polymeric network. The chemical structure of these materials determines the final physical

and mechanical properties of the cured part. Typically, these reactive species consist of moieties that can undergo free-radical polymerization, defined by the presence of unsaturated C=C double bonds. (Meth)acrylate functionalities are commonly used due to their high reactivity when exposed to light and well-established reaction mechanisms. In the commercial market there is a wide range of available (meth)acrylate-based substances suitable for vat polymerization techniques.[30] Among the various options, several commonly employed monomers in light-based 3D printing include 1,6-hexanediol diacrylate (HDDA), polyethylene glycol diacrylate (PEGDA), glycidyl methacrylate (GMA) and butyl acrylates (BA). However, it is important to note that during the polymerization process, there is a possibility of trapping unreacted monomers. As a result, the conversion of the system may not reach 100% and, if it happens, the remaining active species may react with other reactive substances, such as oxygen, which can diffuse within the polymeric network. This phenomenon can lead to aging effects or other alterations in the mechanical and chemical properties of the cured material.[31]

- ***Photoinitiators*** are molecules that, upon exposure to light, absorb photons and undergo a transition to an excited state, resulting in the formation of reactive species that initiate subsequent reactions, after reacting with the double bonds of the monomers.[32] These initiating species can be radicals, cations, or anions: radical photoinitiators are commercially available from various companies, while cationic ones, primarily sulfonium salts, are available in smaller quantities.
  An ideal photoinitiator should possess several key properties, of which the most important are: a high absorption at the specific exposure wavelength and a high molar extinction coefficient; a high quantum yield for the formation of initiating species; the radical generated by the photoinitiator should exhibit high reactivity towards the monomer.[33] Selecting the appropriate photoinitiator is crucial for achieving optimal object fabrication as it directly impacts reaction efficiency and photopolymerization rates, thereby influencing printing resolution and accuracy.[16] It is essential to choose a photoinitiator with an absorption spectrum that aligns with the emission light produced by the printer's light source in order to ensure efficient photopolymerization and to facilitate the desired outcome in the fabrication process.

- ***Additives*** play a pivotal role in tailoring the properties of printable materials and enhancing specific characteristics of both the liquid formulation and the printed object. Among the additives commonly utilized, reactive diluents and dyes or colorants are frequently employed in light-induced 3D printing. *Reactive diluents* are primarily incorporated to adjust the viscosity of the photopolymer within the suitable range for vat polymerization techniques. Additionally, they aid in improving the compatibility among various resin components. The selection of an appropriate reactive diluent depends on several factors, including its affinity with the photopolymer constituents, the desired physical properties of the cured material, the processability of the formulation, and the volatility of the substance.[34] *Dyes* are primarily introduced to regulate light penetration along the Z-axis during 3D printing and enhance printing accuracy in the XY plane.[35] These compounds typically consist of organic molecules, and their selection depends largely on the light source used in the 3D printer. Since incorporating the dye at low concentrations may lead to poor printing resolution and excessively high concentrations can adversely affect the efficacy of the photoinitiator, it is crucial to strike a balance between the dye and other components of the photopolymer. These dyes exhibit specific properties that not only enhance print resolution but also impart distinct characteristics to the printed object.[26]

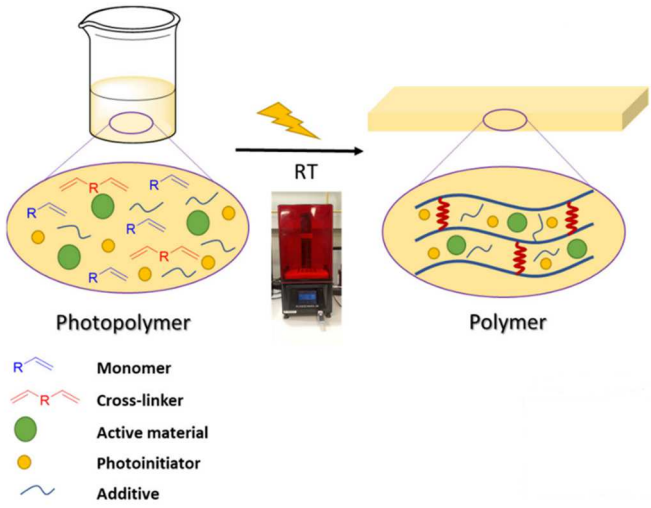

Figure 5 - Representation of the ***Vat Polymerisation process***
Adapted from reference [18]

1.4 - Ionic Liquids

Ionic liquids (ILs) are a unique class of materials with distinct physicochemical properties and fascinating preorganized and adjustable solvent structures. ILs are a class of salts that exist in a liquid state at or near room temperature. Unlike traditional salts, which have high melting points and are typically solid at room temperature, ILs are composed of discrete cations and anions that have been carefully chosen to yield a low melting point (below 100°C) and liquid state. The specific choice of cation and anion can tailor the molecular structure and it influences properties such as viscosity, density, polarity, and solubility, providing researchers with a broad range of options to design ILs with specific characteristics for various applications. Due to their ionic nature, the cations and anions in the liquid are electrically charged species and can facilitate the formation of strong electrostatic interactions within the liquid, which contribute to their stability and unique physicochemical properties, such as:
- ***low volatility***, meaning they have *negligible vapour pressure* at ambient conditions, and ***excellent thermal stability*** allow ILs to be used at elevated temperatures without evaporating, making them ideal for high-temperature applications and harsh reaction conditions; [36]
- ***remarkable solubility*** makes ILs dissolve a wide range of substances, including both organic and inorganic compounds, and attractive for potential applications in the fields of resources, energy, healthcare[37] and CO_2 conversion processes for the past 15 years.[36]

Ionic liquids can also include moieties which can undergo to polymerization and their recent use as precursors, templates, and solvents has resulted in the production of polymeric materials with customized sizes, dimensionalities, morphologies, and functionalities that are challenging to achieve using conventional organic solvents. These polymeric materials obtained from polymerization of ILs are known as poly(ionic liquids) or **polymerized ionic liquids (PILs)**; those are essentially macromolecules composed of ionic groups, which incorporate cationic and/or anionic sites either as pendant groups or within the polymer backbones. Polymerization can be achieved through various techniques, such as free radical polymerization, cationic or anionic polymerization, or ring-opening polymerization. The choice of polymerization method depends on the specific IL monomers and desired properties of the resulting PILs. The transition from ILs to PILs offers several advantages: PILs exhibit enhanced mechanical strength and processability compared to ILs, owing to their polymeric nature; the presence of polymer chains allows for

greater control over the physical and chemical properties of the material, enabling further customization to meet specific application requirements. Their tuneable properties, combined with the inherent advantages of ILs, make PILs versatile materials with potential applications in diverse technological and scientific domains such as catalysis, separation science, energy storage, and materials science.[38]

Ionic liquids have facilitated the conversion of CO_2 into valuable products through various reduction approaches, including chemical, biochemical, photochemical, thermochemical, and electrochemical methods. Among these approaches, the chemical and electrochemical mechanisms have shown significant promise for CO_2 reduction. In the chemical process, CO_2 is converted into carbonates and cyclic compounds through cycloaddition reactions, utilizing epoxides and methanol solvents.[39]

1.5 - Engineering approaches to carbon capture and catalytic valorization

The issue of climate change and the associated increase in CO_2 emissions have emerged as pressing challenges in the contemporary industrial era. With the rapid growth of industrial activities and the burning of fossil fuels, the atmospheric concentration of CO_2 has reached unprecedent levels: considering a global annual emission rate of 40 gigatons and an atmospheric concentration of approximately 3200 gigatons, carbon dioxide emerges as the primary greenhouse gas (GHG).

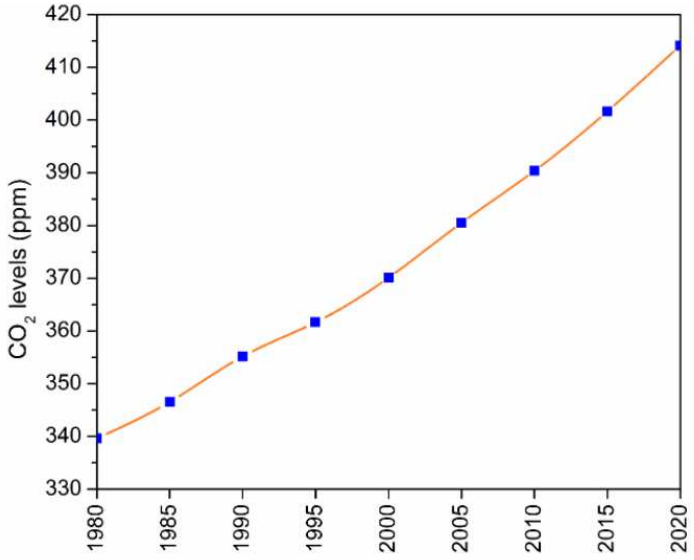

Figure 6 – Increase in CO_2 concentration since 1980s [39]

This rise in greenhouse gas emissions has led to a range of adverse effects, including rising global temperatures, sea-level rise, and extreme weather events. **Figure 6** illustrates the global atmospheric CO_2 concentrations over the years.

To mitigate the impact of climate change, it is crucial to reduce CO_2 emissions and explore innovative approaches, firstly by capturing it and then by storing or using it. In the field of CO_2 capture, there are several engineering approaches that can be categorized into three main categories: **1) Pre-combustion capture** involves capturing CO_2 before the combustion of fossil fuels. This method entails converting the fuel, such as coal or natural gas, into a synthesis gas (a mixture of carbon monoxide and hydrogen) through chemical reactions like gasification or methane reforming. The synthesis gas is then subjected to a separation process to remove CO_2 before it is burned. This approach allows for higher CO_2 concentrations, facilitating subsequent capture. **2) Post-combustion capture**, on the other hand, involves capturing CO_2 from the flue gases produced by the combustion of fossil fuels. After combustion, the flue gases pass through a separation process where CO_2 is captured using a chemical solvent or porous material. Solvent-based absorption, such as amine scrubbing, is commonly employed in post-combustion capture. Once captured, the CO_2 can be compressed, transported, and stored in underground reservoirs or utilized for other applications. **3)** *Combustion capture* involves capturing CO_2 during the combustion of fossil fuels. One promising method in this domain is **Oxyfuel combustion**, where pure oxygen is used instead of air for combustion. This results in flue gases mainly composed of CO_2 and water vapor. CO_2 can be separated from the water vapor relatively easily compared to air-based flue gases and, once captured, can be further processed and stored or used for industrial purposes.[39]

In addition to CO_2 capture, one prominent strategy for its subsequent management is ***carbon capture and storage (CCS)***, that has emerged as one of the primary strategies for addressing this issue. CCS involves the capture of CO_2 emissions from various sources, such as power plants or industrial processes, followed by its transportation and secure storage deep underground or its utilization in industrial applications. This process prevents a significant amount of CO_2 from being released into the atmosphere, mitigating its contribution to global warming. [39], [40] Another available solution is ***carbon capture and utilisation (CCU)***, in which carbon dioxide is viewed as a valuable resource for the chemical or biological synthesis of commercially significant chemicals and fuels, rather than being treated as waste. This paradigm shift transforms carbon dioxide into a valuable chemical feedstock and embodies a transition from a linear to a circular economy approach in energy and

chemicals production. By harnessing carbon dioxide in this manner, CCU represents a sustainable process with the potential to contribute to a more environmentally conscious and efficient utilization of resources.[41]

The conversion of carbon dioxide into chemicals encompasses a diverse range of processes, resulting in various products, such as urea, salicylic acid and cyclic carbonates. For example, the production of ***urea*** through the reaction between carbon dioxide and ammonia has been commercially practiced since 1921 and is presently the largest-scale chemical synthesis, yielding approximately 150 million tonnes of urea annually. The synthesis of ***salicylic acid*** from phenol and carbon dioxide under basic conditions is another well-established process, that dates back to 1890 and serves as the initial step in the industrial production of aspirin. The spontaneous formation of urea and salicylic acid from carbon dioxide occurs in the absence of a catalyst.

In contrast, the reaction between carbon dioxide and epoxides (**Figure 7**), from which ***cyclic carbonates*** can be produced, is known as **cycloaddition reaction** and necessitates the presence of a catalyst and can be tailored to yield either a cyclic carbonate or a polycarbonate. This commercial production, dating back to 1958, finds application in numerous industrial uses, such as electrolytes in lithium-ion batteries, polar aprotic solvents, and gas separations.[41], [42] In this context, by employing 3D printing techniques it is possible to develop advanced catalytic systems, that play a vital role in the valorization of captured CO_2, and then to create complex and precisely engineered structures, tailoring the catalytic reactor's properties and enhancing its performance.[43]

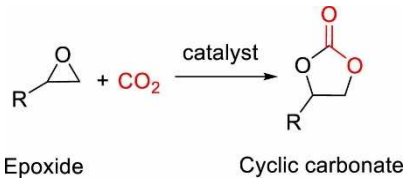

Figure 7 - Cyclic carbonate synthesis [42]

Several examples of cycloaddition reactions using ionic liquids as solvents and catalysts can be found in the literature. These examples demonstrate the potential of ionic liquids to facilitate the conversion of CO_2 and epoxides into cyclic carbonates. Here are some notable examples:

1 – One of the first utilizations of ionic liquids (ILs) as catalysts for the conversion of CO_2 to cyclic carbonate was documented by *Peng and Deng in 2001 (*[44]*)* . In their

study, they successfully synthesized propylene carbonate (PC) using conventional ILs. The IL employed in their research comprised imidazolium and pyridinium cations, combined with anions such as chloride (Cl^-), tetrafluoroborate ($BF4^-$), and hexafluorophosphate ($PF6^-$). The experimental results demonstrated the efficacy of this conventional IL in facilitating the desired transformation, thus highlighting its potential for CO_2 utilization in cyclic carbonate synthesis and with the imidazolium-based ILs achieving an impressive yield of 90% for PC.[45]

2 – In another research paper, apart from imidazolium-containing ionic liquids, the efficient activation of CO_2 into cyclic carbonate has been reported using quaternary ammonium salts, as demonstrated by *Calo et al. (*[46]*).* In their study, the synthesis of cyclic carbonate under a CO2 atmosphere was promoted using tetrabutylammonium halides salt (TBAX). Furthermore, they investigated the nucleophilicity effect of bromide (Br^-) or iodide (I^-) anions on the activity of carbonate synthesis and proposed a mechanism for the reaction.[45]

3 – Another example can be found in the works of *Sun et al.* [47] and *Wang et al.* [48]. They investigated the use of specific ionic liquids (ILs), namely 1-(2-Hydroxyethyl)-3-methylimidazolium bromide [HEMIm]Br and 1-Butyl, 2-hydroxymethyl, 3-methylimidazolium bromide [BHMMIm]Br, for the synthesis of cyclic carbonates. Notably, these ILs demonstrated remarkable performance, yielding propylene carbonate (PC) with exceptional efficiency (up to 99%) under mild operating conditions and short reaction times. Furthermore, the studies provided insights into the catalytic mechanism, revealing the ILs' dual functionality as bi-functional catalysts. This involved the activation of the epoxide through hydrogen bonding (OH and epoxide O) and the nucleophilic attack of a Lewis basic B species.[45]

The findings from these studies contribute to the expanding knowledge base on CO_2 utilization and offer valuable insights for the development of efficient and sustainable processes for cyclic carbonate synthesis.

Furthermore, on the synthesis of cyclic carbonates through the mentioned reaction is based one of the potential applications of 3D printed catalytic reactors obtained in this research and printed with stereolithography technique, after optimizing their design, composition and printing parameters.

2. EXPERIMENTAL METHODOLOGY

2.1 – Materials

All reagents and solvents used during this work were commercially available: Glycidyl methacrylate (97%, Aldrich), **GMA**; 1,4-Butanediol diacrylate (90%, Aldrich), **BUDA**; Pentaerythritol Tetraacrylate (>99%, Aldrich), **PETA**, Phenylbis(2,4,6-trimethylbenzoyl) phosphine oxide (97%, Aldrich), **BAPO**; Methyl Red (ACS reagent, crystalline, Aldrich), **MR**; Pentaerythritol tetrakis (3,5-di-tert-butyl-4-hydroxyhydrocinnamate) (98%, Aldrich), **Radical Scavenger**; Poly(ethylene glycol) diacrylate, **PEGDA**, with an average molecular weight of 250 g/mol; ink (ELEGOO translucent LCD UV-Curing). The chemical structures[2] of the components are illustrated below in **Errore. L'origine riferimento non è stata trovata.**.

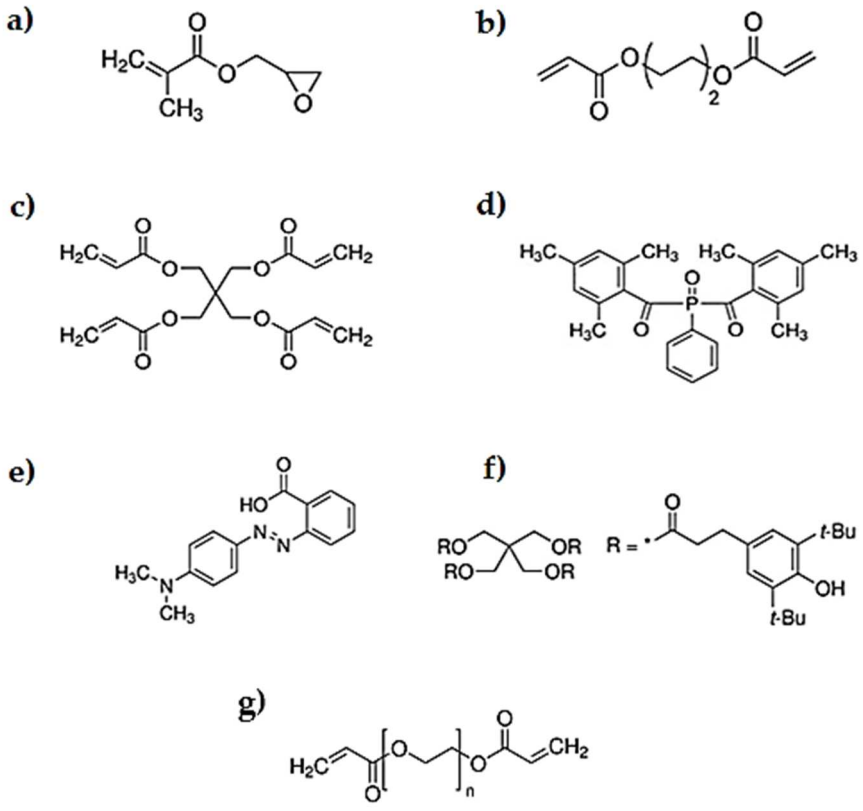

Figure 8 - Chemical structures of (a) **GMA**, (b) **BUDA**, (c) **PETA**, (d) **BAPO**, (e) **MR**, (f) **Radical Scavenger**, (g) **PEGDA**

[2] Structure taken from the monomer manufacturer's website [49]

2.2 - Formulations developed

3DP-F1 composition: The printer tank was filled with 50.0 mL a monomeric solution containing 50% by weight of GMA, 50% by weight of BUDA, and 2 wt% of the photoinitiator (Phenyl-bis-(2,4,6-trimethylbenzoyl)phosphine oxide) regarding the monomers, 0,1 wt% Pentaerythritol tetrakis (3,5-di-tert-butyl-4-hydroxyhydrocinnamate) and 0,1 wt% Methyl Red. The 3D structure was obtained according to the digital design downloaded in the printer (short fusilli with different helix pitches).

3DP-F2 composition: The printer tank was filled with 50.0 mL a monomeric solution containing 60% by weight of GMA, 40% by weight of PETA, and 2 wt% of the photoinitiator (Phenyl-bis-(2,4,6-trimethylbenzoyl)phosphine oxide) regarding the monomers, 0,1 wt% Pentaerythritol tetrakis (3,5-di-tert-butyl-4-hydroxyhydrocinnamate) and 0,1 wt% Methyl Red. The 3D structure was obtained according to the digital design downloaded in the printer (reactors R1, R2 and R3[3]).

FORMULATIONS	**GMA**	**CROSS-LINKER**	**PHOTOINITIATOR**	**ADDITIVES**	
3DP - F1	50% wt.	50% wt. BUDA	2% (*) wt. BAPO	0.1% (*) Metyl Red	0.1% (*) Radical Scavenger
3DP - F2	60% wt.	40% wt. PETA			

(*) regarding the total mixture of GMA and Cross-linker

Commercial Resin (3DP-COMM): The printer tank was filled with 50.0 mL Standard Translucent Photopolymer Resin. The 3D structure was obtained according to the digital design downloaded in the printer (reactors R1, R2 and R3).

2.3 - Equipment

3D printers - A DLP printer (***Asiga MAX27-UV***)[4] and a MSLA printer (***Elegoo Mars 3***)[4] were the 3D printers employed (**Figure 9**). The DLP printing system was equipped with a LED light source operating at 385 nm and a 62 μm pixel resolution. The Elegoo Mars 3 printer was equipped with a 4098 × 2560 mono liquid crystal display (LCD), illuminating at 405 nm. The CAD files were designed and converted to STL-type files using **SolidWorks CAD software**. The digital light processing fabrication in both printers began by slicing the 3D CAD model into individual 2D images for projecting onto the photocurable liquid.

[3] Shape shown in **Figure 15** in ***3.1.1 Solidworks design***

[4] From technical data sheets of the two printers [50], [51]

For Asiga MAX27 - UV printer, the additive manufacturing software used to create slices was Asiga Composer. For the Elegoo Mars 2 Pro 3D printer the slicer software employed was ChituBox.

Figure 9 - **3D printers**: (Left) ***Asiga MAX 27-UV***; (Right) ***Elegoo Mars 2 Pro***

Fourier Transform Infrared (***FT-IR***) spectra were acquired with a Pike single-reflection ATR diamond/ZnSe accessory in a JASCO FT/IR-4700 instrument in transmission mode averaging 8 scans for each spectrum in a wavenumbers' range of 600 – 4000 cm^{-1}. FTIR spectroscopy is employed to examine the absorption properties of a sample within the mid-infrared range of the electromagnetic spectrum (4000 - 500 cm^{-1}). Each functional group exhibits a unique absorption pattern at a specific wavelength, enabling the analysis of spectral bands to provide insights into the sample's chemical composition. When operating in absorbance mode, the intensity of these bands allows for quantitative measurements. Through Fourier transform operations, the initial raw data is transformed into a final spectrum consisting of multiple peaks, where the intensity of absorption is associated with changes in the dipole moment of molecules. To analyze the surface-level properties of samples rather than the entire bulk material, an attenuated total reflectance (ATR) accessory is utilized. In this configuration, the IR signal slightly penetrates the sample's surface, reaching depths of approximately 1 - 2 micrometers. In this study, FTIR spectroscopy is employed to characterize the samples by monitoring the changes in peaks corresponding to specific functional groups.

*Thermal Gravimetric Analysis (**TGA**)* & *Differential Scanning Calorimetry (**DSC**)* were performed on TGA-DSC3 analyser from Mettler Toledo. ***TGA*** is a thermal analysis technique that measures the change in mass of a sample as a function of temperature or time under controlled heating conditions. During the analysis, a small sample is heated in an inert or oxidizing atmosphere, and the weight change is continuously recorded by a sensitive balance. The resulting thermogram provides information on the sample's thermal behavior, including degradation temperature, decomposition pathways, and thermal stability. ***DSC*** is a widely employed technique to investigate the thermal properties of materials. It measures the difference in heat flow to or from a sample and an inert reference material as a function of temperature. During DSC analysis, both the sample and reference material are subjected to the same heating or cooling program, and any heat absorbed or released by the sample is detected by a highly sensitive calorimeter. The resulting DSC curve provides information on endothermic and exothermic transitions, such as melting, crystallization, glass transitions, and chemical reactions. Samples for TGA and DSC analysis were heated in an inert atmosphere from room temperature to 700 ˚C with a heating rate of 15°C/min. The initial degradation temperature (T_0) was obtained at 5% of mass loss.

*X-ray photoelectron spectroscopy (**XPS**)* - A PHI 5000 Versaprobe scanning X-ray photoelectron spectrometer was used in the investigation of the surface chemical characteristics of 3D printed samples in disc shape. The instrument featured a monochromatic Al K-α X-ray source with an energy of 1486.6 eV, a voltage of 15 kV, and an anode current of 1 mA. For data collection, a spot size of 100 mm was employed to capture the photoelectron signal for both high-resolution (HR) and survey spectra. To ensure accurate measurements, different pass energy values were utilized: 187.85 eV for survey spectra and 23.5 eV for HR peaks. To mitigate the charging effect during measurements, all samples underwent analysis with a combined electron and argon (Ar) ion gun neutralizer system. The core level peak energies were referenced to the C1s peak at 284.5 eV, and a Shirley function was applied to subtract the background contribution in HR scans[52]. XPS is a non-destructive technique that utilizes X-ray radiation to probe the electronic structure of a material's surface. When X-rays are directed onto a sample, the X-ray photons interact with the surface atoms, causing the emission of photoelectrons. These emitted photoelectrons carry information about the binding energies and kinetic energies of the electrons within the material. By analyzing the energies of these photoelectrons, valuable insights can be obtained regarding the elemental composition, chemical states, and surface chemistry of the material. Data analysis was carried out using the dedicated software Multipak 9.6. Furthermore, a depth profile was conducted using an alternate mode, employing sputtering cycles of 1 minute each, facilitated by ionized argon (Ar+) flux at an accelerating voltage of 2 kV.

3D Scanning - To assess the printing fidelity and compare the printed geometry with the CAD design, a 3D scanner was employed. Specifically, the ***3Shape E4 scanner*** (3Shape A/S, Copenhagen, Denmark) was utilized, which features four 5 MP cameras and boasts a measurement accuracy of 4 μm. The analysis of the scanned data was conducted using the Convince software developed by 3Shape. In the scanning process, the sample was coated with a thin layer of talc and positioned on the scanner platform. The resulting image captured by the scanner was then compared with the original CAD file to generate a colorimetric map, enabling a visual evaluation of the deviations between the printed object and the intended design.

Elemental Analysis - The ***CHN628 Elemental Analyzer*** with an additional S module from Leco was utilized for elemental analysis. It offers high precision, accuracy and has a high capacity for handling macro masses, for example, 750 mg for solids and up to 1 mL for liquids, providing results for all determined elements in just 4 or 5 minutes. Elemental analysis allows for the determination of C, H, N, O, and S in materials of various origins, typically organic, achieved by combusting the sample within a high-temperature furnace. The resulting gases are then carried with helium through reagents that reduce the number of gaseous species in the combustion mixture. Subsequently, they pass through a thermal conductivity detector, which measures N_2, and high-sensitivity infrared detectors, which determine CO_2, H_2O, and SO_2. Based on these measurements, the content of N, C, H, O, and S in the sample can be evaluated.

Swelling - Fusilli-shaped samples were placed in different solvents with a sufficient amount to make them totally submerged and left to soak for 24 hours at room temperature. The degree of swelling in the solvents, expressed as a percentage (S_w%), was calculated by measuring the weight change between the swollen sample (W_s) and its initial weight (W_i).

$$Sw\% = \left(\frac{W_s - W_i}{W_i}\right) * 100 \quad (1)$$

Another type of swelling analysis was calculated and utilized, focusing on the dimensions of the samples. This analysis aimed to determine the extent to which the original dimensions needed to be reduced in order for the printed object to be suitable for subsequent reactions while maintaining the required dimensions. The formula used for this analysis was the same as the one mentioned above, with the weight values replaced by the values of various dimensions such as length and diameter. The resulting value represents the percentage of swelling based on dimensions (S_d%).

$$Sd\% = \left(\frac{D_s - D_i}{D_i}\right) * 100 \quad (2)$$

Nuclear Magnetic Resonance (***NMR***) *Spectroscopy* - The conversion of CO_2 cycloaddition reactions was determined through the analysis of ^1H NMR spectra, which were acquired using a Bruker Avance III HD 300 or 400 spectrometer (operating at either 300 or 400 MHz for ^1H). By examining the chemical shifts and peak intensities in the NMR spectra, the extent of conversion for the cycloaddition reactions involving CO_2 could be accurately evaluated.

2.4 - 3D printing procedures

Even if SLA and DLP 3D printers were used, the process of obtaining a 3D printed involved the same several fundamental steps. It began with the creation of a 3D model using *Solidworks* as CAD software, ensuring that it is then converted into the STL file format. The next step involved importing this file into the specialized slicing software with which the printer was equipped: it enabled the division of the 3D model into a series of thin horizontal layers and the setting of the printing parameters, like layer thickness, exposure time and light intensity, that had to be adjusted in order to optimize print quality, speed and material usage; furthermore, it allowed the creation of the required supports for overhanging or intricate features to ensure successful printing.

In both SLA and DLP processes, the initial layers required longer exposure times compared to the subsequent layers for several reasons. At the beginning of the printing process, when light was projected onto the photosensitive resin, which was in contact with the build platform or the bottom surface of the vat, the process of polymerization took place, gradually solidifying the liquid resin layer by layer to create the three-dimensional object. During the exposure of the first layers, also called *burn-in layers*, it was crucial to ensure that the entire area of the layer was fully polymerized: it needed a longer exposure time to ensure that every point of the first layers was adequately exposed to the light, avoiding the formation of weak or under-cured spots that could have compromised the stability and integrity of the printed object. Furthermore, the initial layers were typically more critical in terms of adhesion to the build platform or the bottom surface of the vat. Longer exposure helped to ensure that the first layer securely bonded to the platform or vat surface, providing a solid foundation for the subsequent layers. As the printing progresses and subsequent layers were overlaid onto the first layer, the developing three-dimensional object gained stability and support from the underlying layers. This

reduced the need for extended exposure times as the subsequent layers could benefit from the support provided by the previously solidified layers.

Once the model was prepared, the sliced file was exported in G-code format, containing then the instructions for the 3D printer. With the printer properly set up, including a clean and level build platform and the appropriate photocurable resin in the vat, the printing process can be initiated. During the printing process, the SLA or DLP printer followed the instructions provided in the *G-code file*. Using either a laser (SLA) or a digital light projector (DLP), the printer selectively cured the liquid resin layer by layer until the printed object was formed. After the printing was completed, post-processing steps were carried out to finalize the printed object, such as removing the object from the build platform or the resin vat, washing it with IPA (3 x 25 mL) to remove any uncured resin and post-curing at 60 °C for 15 min under UV lamp.

2.5 – Functionalization of the 3D printed materials

Functionalization refers to the process of modifying a material or surface by introducing specific functional groups or chemical moieties onto its structure. This modification aims to impart new properties or functionalities to the material, enabling it to interact with other substances or exhibit desired behaviours. It can involve various techniques such as chemical reactions, surface coatings, or attachment of functional molecules or polymers. Its purpose is to tailor the material's surface or bulk properties to meet specific requirements, such as improved adhesion, enhanced reactivity, biocompatibility, or selective targeting in various applications ranging from nanotechnology and electronics to biomedicine and catalysis.[53]

In this work the functionalization was made through the nucleophilic ring opening of epoxides in the presence of a solution of the chloride salt of butyl imidazole (6.5 M) in a solvent, as reported in literature [54]. The 3D printed object was placed in a beaker, which was then placed on ice. Hydrochloric acid and solvent were sequentially added to the beaker, followed by the careful addition of drops of butyl imidazole, or in other cases all together. However, it was crucial to ensure the correct molar quantities (6.5 mmol of butyl imidazole and 6.5 mmol of hydrochloric acid in 1 ml of solvent) to cover the entire object. After removing the beaker from the ice, the object was left immersed in the solution at a temperature of 40 or 60 °C on a magnetic stirrer (260 rpm) for a duration of 24 hours. Once the required 24-hour period had elapsed, the object was washed with isopropanol (IPA) in three consecutive cycles of 25 ml each and subsequently dried at 60°C under vacuum for another full day.

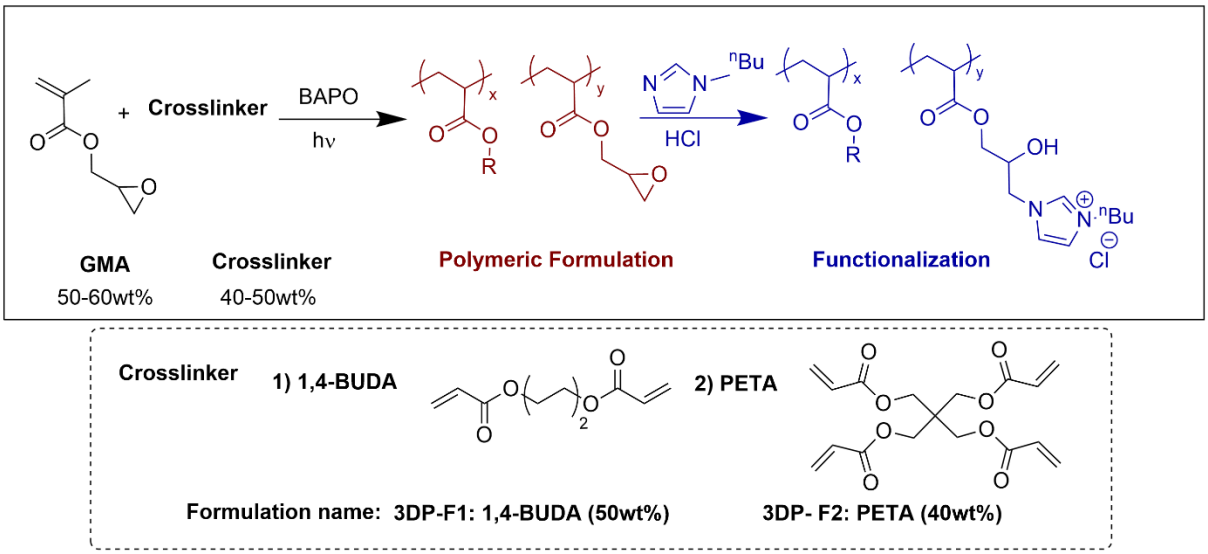

Figure 10 - Chemical structure of the formulation prepared for this work

2.6 - Materials for functionalization

Hydrochloric acid (HCl, 37% - Scharlau) is a strong inorganic acid commonly used in various chemical reactions and laboratory procedures. It is highly corrosive and possesses the ability to donate a proton (H+) in aqueous solutions. In the context of the functionalization process based on epoxy ring opening, hydrochloric acid is utilized to facilitate the opening of the epoxy ring and initiate the desired chemical reaction.

Butyl imidazole (1-Butylimidazole, > 98% - TCI) is an organic compound that belongs to the imidazole family. It is used as a catalyst or reagent in various chemical transformations, including the functionalization of materials. Butyl imidazole is employed in the functionalization process to react with the opened epoxy ring, forming covalent bonds with the material's surface and introducing specific functional groups.

Ethanol (Ethanol absolute, ≥ 99.8% - VWR Chemicals), also known as ethyl alcohol (***EtOH***), is a volatile organic compound commonly used as a solvent or reagent in chemical processes. It is miscible in water and has a wide range of applications. In the functionalization procedure, ethanol serves as a solvent to dissolve both hydrochloric acid and butyl imidazole, enabling their effective mixing and subsequent reaction with the material's surface.

The chemical structures of Butyl imidazole[5] and ethanol are illustrated below in **Figure 11**.

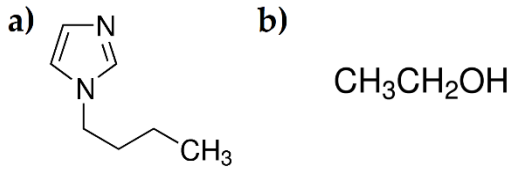

Figure 11 - Chemical structure of (a) **Butyl Imidazole** and (b) **EtOH**

2.7 – CO_2 cycloaddition

One of the focal points of this work was the application of the 3D printed materials as reactors for the CO_2 cycloaddition to epoxides to produce cyclic carbonates, building upon previous research [54], in which 3D-printed reactors with specific designs were utilized to evaluate their impact on the reaction. After optimizing the formulation to achieve excellent printing resolution and designing and printing new fusilli-shaped structures, the reactors were incorporated into a commercially available Omnifit™ column, measuring 15 cm in length and 1 cm in diameter, enabling their utilization under continuous-flow conditions (**Figure 12**). To enhance mechanical strength and ensure optimal flow distribution, four thin pillars were added to the initial design (the reactors R1 and R2 with different pitch, 4 mm and 2.5 mm respectively, are shown in **Figure 15**). These modifications improved the resistance and durability.

Figure 12 - Reactors in ***Omnifit™ column***: (left) **R1** before reaction; (right) **R2** during the reaction

[5] Structure taken from the manufacturer's website [55]

In a standard catalytic reaction procedure, a mixture comprising 1.0 mmol (0.120 g) of ***styrene oxide***, 2 mmol (0.644 g) of ***Tetrabutylammonium Bromide*** (**TBA.Br**), 16 mL of ***Acetonitrile***, and 4 mL of H_2O was continuously pumped using an HPLC pump at a flow rate of 0.05 mL/min. Simultaneously, CO_2 was also pumped with a peristaltic pump (nominal flow rate of 0.20 mL/min at 6.5 bar pressure) and mixed with the liquid phase using a T-mixer. To account for gas compression and solubility in the solvent at a temperature of 25°C, the effective CO_2 flow rate was determined to be 41 µL/min. The reaction took place inside a column reactor containing the 3D-printed structure and was conducted at a temperature of 100°C and a pressure of 6 bar. The 3DP structured reactors R1 and R2 performance was compared to archetypal continuous-flow reactors, i.e. a packed-bed reactor (PBR) and a coiled reactor [56]. The residence time varied depending on the reactor structure employed, with values ranging from 47 to 60 minutes (R1 = 47 min; R2 = 51 min; PBR = 55 min; coil = 60 min). The conversion and selectivity of the products were determined by ^{1}H NMR spectroscopy, allowing for quantitative analysis of the reaction outcomes. Here below it is shown how residence time, productivity, conversion and selectivity were calculated.

The **residence time** was determined using this equation:

$$Residence\ time\ (t) = \frac{Vr(mL)}{Q\left(\frac{mL}{min}\right)} \tag{3}$$

Here *Vr* represented the volume of the reactor (R1 = 4.30 mL; R2 = 4.63 mL; PBR = 5.46 mL; coil = 5 mL), Q denoted the flow rate, calculated by summing up the flow rate of gas (experimentally determined) and liquid.

The **productivity** was calculated using the equations:

$$Productivity\ (P) = \ Q\left(\frac{mL}{h}\right) * C\left(\frac{\mu mol}{mL}\right) * \frac{Y}{100} = \left[\frac{\mu mol}{h}\right] \tag{4}$$

$$Normalized\ Productivity\ \ (NP) = \ P\ \left(\frac{\mu mol}{h}\right) * \frac{t_r}{t_{rm}} = \left[\frac{\mu mol}{h}\right] \tag{5}$$

In these equations, C was the concentration of the solution, Y corresponded to the yield of the reaction (mol product/mol limiting reagent, obtained by multiplying the selectivity by conversion), t_r meant residence time of the reactor (R1 = 47 min; R2 = 51 min; PBR = 55 min; coil = 60 min), t_{rm} represented the minimum residence time between the tested reactors (R1= 47 min).

Additionally, considering that the *total number of moles of all the products* was given by the sum of the *cyclic carbonates' moles and* the *by-product's moles*, the **conversion** and the **selectivity** of the reaction were calculated as follows:

$$Conversion\ \% = \frac{mol\ of\ products}{mol\ total} * 100 \quad (6)$$

$$Selectivity\ \% = \frac{mol\ of\ cyclic\ carbonate}{mol\ of\ products} * 100 \quad (7)$$

3. RESULTS AND DISCUSSION

3.1 – 3D printing

3.1.1 Solidworks design

To commence the 3D printing process, the CAD model with the desired geometry was carefully chosen and developed using Solidworks software. Several geometries were designed for subsequent printing using specially formulated resins, customized specifically for the selected 3D printer, instead of relying on commercially available resins. Given that one of the intended applications for this research project involved the incorporation of structures into flow columns for carbon dioxide conversion, diverse objects with distinct shapes were created, as depicted in **Figure 13**.

Figure 13 - ***3D structures***: (left) **fusillo**, (centre) **gyroid**, (right) **lidinoid**

A different structure, called the Benchmark, was then employed to evaluate the resolution of various formulations. As shown in **Figure 14**, this structure consists of small pillars and walls with varying thicknesses (2, 1.5, 1, 0.5, and 0.25 mm).

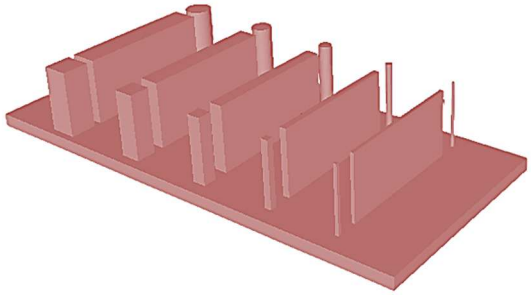

Figure 14 - **Benchmark** 2_1.5_1_0.5_0.25 mm

After identifying the optimal formulation and structure for further research, efforts were made to optimize the structure itself. Initially, modifications were made to the helix pitch, followed by the incorporation of slender columns within the structure to improve both its strength and flow conditions. Presented below in **Figure 15** are three additional steps undertaken to modify the structure.

Figure 15 - Fusilli's structure with helix pitch of **4**, **2.5** and **1.8** mm, called **R1**, **R2** and **R3** respectively.

3.1.2 Development of formulations

In this work two different polymeric formulations have been employed, both based, at first, on the commercial monomer *Glycidyl Methacrylate (GMA)*, that was considered as a viable functional monomer in the pursuit of a straightforward and simple approach to fabricating functionalized additive manufacturing polymeric devices. GMA demonstrates copolymerization capabilities with various conventional monomers, providing a cost-effective method to incorporate reactive functional groups into polymeric matrices. This facilitates post-functionalization of the polymer for diverse application purposes.[54]

For each polymeric resins a different additional cross-linker was used in order to evaluate its impact on the polymeric backbone and to precisely tailor the mechanical characteristics of the resulting materials. Two distinct acrylate-based and reactive compounds were tested as supplementary cross-linkers for this purpose: *1,4-Butanediol Diacrylate (BUDA)* and *Pentaerythritol Tetraacrylate (PETA).* In both monomeric mixtures *Phenylbis(2,4,6-trimethylbenzoyl)phosphine oxide (BAPO)* was added as a photoinitiator, but in different percentages.

This study started with a base formulation used in *Valverde et al.*'s research [54], which was optimized to partially eliminate the use of a commercially available photopolymer resin provided by the printer manufacturer (in this case, the Elegoo Mars 3). The initial polymer resin, used exclusively for printing the spiral-shaped structure, consisted of 50% **GMA** and 50% **BUDA** by weight. As the first modification, **BAPO** was added as a photoinitiator at a concentration of 0.5% w/w, regarding the total amount of GMA and BUDA. However, the initial results of

printing the spirals with a 2.5 mm pitch did not meet the expected resolution, as shown in **Figure 16**. The achieved resolution was significantly lower compared to the CAD file. To achieve the desired resolution, further attempts were made by gradually increasing the weight percentage of the photoinitiator up to 1.5%, in steps of 0.5%. This led to a slight improvement in detail, such as increased spacing between the helices, but the quality of overall structure worsened. The structures depicted in **Figure 16** are incomplete since the printing process was interrupted to assess the obtained results, revealing the above-mentioned problems.

Figure 16 - Formulation development increasing BAPO quantity:
(*left*) **0.5% wt.**, (*centre*) **1% wt.**, (*right*) **1.5% wt**.

Noticing that 3D printed objects could still be obtained, efforts were made to modify the printing parameters. The steps taken and illustrated in **Figure 17** involved increasing the photoinitiator concentration to 2% by weight. Initially, it was decided to reduce the exposure times by a few seconds compared to the optimization carried out by *Valverde et al.* [54], as BAPO was added to facilitate photopolymerization. The initial attempts were executed with an exposure time of 21s for the first 8 layers, followed by 17s for the subsequent layers (all the layers had a thickness of 0.05 mm), gradually decreasing layer by layer as programmed by the printer. Despite the addition of 2% BAPO by weight, the desired resolution was still not achieved. Two further modifications were implemented, increasing the exposure times to 24s for the burn-in layers and 20s for the subsequent layers. Additionally, a 2.5-second waiting time was introduced for the printer's head at the highest point before descending back into contact with the polymer resin. This allowed the resin to have more chances of not remaining attached to the structure before the polymerization of the next layer. However, this led to an over-exposure situation where the central part of the structure solidified to a greater extent, resulting in insufficient free space between each helix, as observed in the CAD structure. Therefore, the exposure times were lowered again, setting them at **22s** and **18s**, respectively, for the ***burn-in layers*** and the ***subsequent layers***, while maintaining the same waiting time. This adjustment

finally achieved a level of resolution close to the desired target but not yet fully comparable.

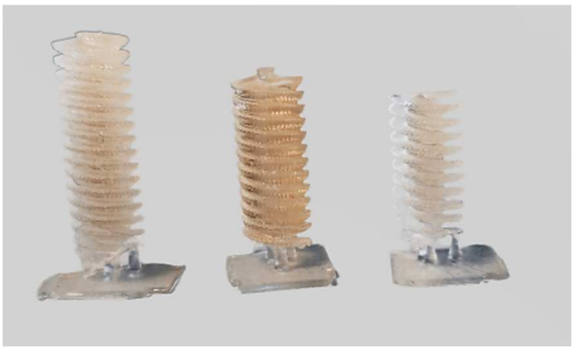

Figure 17 - Formulation development adjusting printing parameters:
(left) **21s/17s**; (centre) **24s/20s**; (right) **22s/18s**.

With this formulation the main problem was to achieve a good resolution of the 3D printed object. For this reason, a dye, *Methyl Red (MR)*, and a radical scavenger, *Pentaerythritol tetrakis (3,5-di-tert-butyl-4-hydroxyhydrocinnamate)*, were both added in a small percentage (**0.1% w/w**, regarding GMA and BUDA). In this case there was no improvement such as to obtain optimal resolution. On the contrary, there was a visible worsening in resolution. In this case it was not possible to obtain solid structures, but rather structures with viscous helix sides that were never completely polymerised (**Figure 18**), even increasing exposure times. As mentioned above in the "**2.2- Formulations developed**" section, this formulation was named **3DP-F1.**

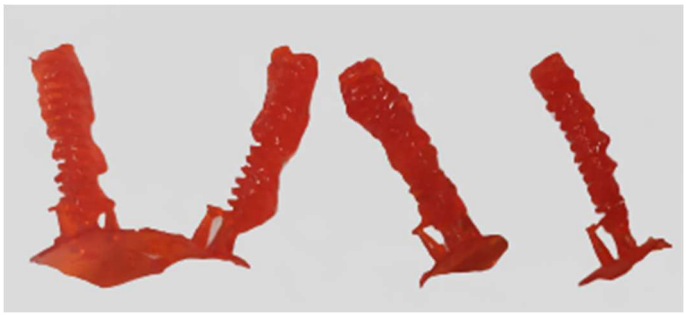

Figure 18 - Not polymerised fusilli using **3DP-F1**

Once it was determined that the desired resolution for constructing the spiral-shaped structure could not be achieved with the current formulation, even with the addition of additives, a decision was made to switch to a new formulation, that was optimized using the DLP 3D printer, *Asiga MAX27-UV*. The goal was to replace the cross-linker with another multifunctional monomer, to achieve earlier gelation a thus better

controlling polymerization. At the same time, it was increased the weight percentage of GMA, to maximize the amount of epoxy groups, which would be essential for achieving a higher quantity of PILs on the structure's surface after functionalization. Initially, two formulations were made, both consisting of 70% GMA by weight, with the remaining 30% containing a different cross-linker, such as pentaerythritol tetraacrylate (PETA) and dipentaerythritol penta-/hexa-acrylate. The first formulation with PETA was chosen because it exhibited better solubility in GMA. In this case, the printing process was directly attempted for the 'Benchmark' structure, incorporating 2% BAPO by weight, regarding the total amount of GMA and PETA, from the beginning. However, this formulation failed to produce any constructive results, as no adhesion to the printer's head was achieved despite adjusting the printing parameters. Consequently, a different approach was adopted, combining two distinct compositions: the first composition consisted of ***Poly(ethylene glycol) diacrylate*** (*PEGDA*), with an average molecular weight of 250 g/mol, and BAPO 1% w/w and it was made to ensure ease of printability and facilitate adhesion of the initial layers to the build platform in order to have a solid base (since it was easier to print with PEGDA, the *layer thickness* was set at ***0.1 mm***); the second composition remained identical to the previous one with *layer thickness* of ***0.05 mm***.

In this case, only the three thickest parts of the 'Benchmark' structure with 2 mm, 1.5 mm and 1 mm thickness could be successfully printed by adjusting parameters such as the exposure times for the burn-in and subsequent layers and the light intensity. Subsequently, another modification was made to the weight percentages, with GMA and PETA adjusted to 60%wt./40%wt. With this formulation, four out of the five parts of the 'Benchmark' structure were printed, excluding the thinnest part. A printable thickness of 0.5 mm was achieved using the same parameters that yielded the best results for the 70%wt./30%wt. composition (exposure time of **3.5s** for the ***'burn-in' layers*** made with PEGDA, exposure time of **5s** for the ***subsequent layers***, *waiting time* after exposure of **0.5s** and maximum ***light intensity*** set at **49 mW/mm²**). Building upon this formulation, an attempt was made to print a gyroid structure, which yielded positive results with a reasonably good print resolution (**Figure 19**). This success paved the way for further optimization of the formulation.

Figure 19 - 3D printed Gyroid with 60% w/w GMA, 40% w/w PETA and 2% w/w BAPO, regarding both GMA and PETA

Afterwards, to further improve the resolution, enhance the printing process and achieve better results, the *same* ***dye*** and the *same* ***Radical Scavenger***, as it happened in ***'3DP-F1'***, were added to the formulation, each at a **0.1% w/w**, relative to the total amount of GMA and PETA. In particular, *Methyl Red* could assist in visualizing the printed structure and evaluating the quality of the printed layers and the *radical scavenger* helped to mitigate unwanted polymerization reactions, leading to improved print fidelity and resolution. The incorporation of these additives at a 0.1% weight percentage was found to be effective in producing successful prints of the gyroid, fusilli, and lidinoid objects, with the necessary supports to maintain their attachment to the printer platform (**Figure 20**). As mentioned above in the "**2.2-Formulations developed**" section, this formulation was named '**3DP-F2'.**

Figure 20 - 3D printed structures with '**3DP-F2**'

After observing that achieving the desired resolution level was more challenging for the gyroid and lidinoid structures (e.g., certain holes visible throughout the CAD file were not apparent), the decision was made to continue focusing on the fusilli structures due to their successful printing performance (**Figure 21**). However, difficulties arose when attempting to print the fusilli vertically. This change in printing orientation was implemented to minimize the need for supports for two reasons: firstly, to ensure the highest-quality structure, avoiding significant fractures during support removal, and secondly, to align with a potential subsequent application that required a well-defined vertical structure for easy insertion into a flow column. Consequently, further optimization of the printing parameters was necessary.

Figure 21 - Fusilli printed **horizontally** with '**3DP-F2**'

Achieving vertical printing of the fusilli structures proved to be more challenging due to several factors that needed consideration. For instance, the increased weight that had to be supported by a reduced number of supports posed a challenge. In initial attempts with low exposure times, the resin failed to undergo photopolymerization. Subsequent attempts with longer exposure times of 3 or 4 seconds resulted in potential resin entanglement within the spiral structure during the printing of successive layers.

An intermediate solution was devised, which proved highly effective. It involved adjusting the printer's light intensity to a lower setting but using longer exposure times (for the 3DP-F2 resin), divided into thickness ranges of 2 mm. Towards the end of each range, the exposure times were slightly decreased. Additionally, the printer was operated within the UV protection cover of the printer at a temperature of 30°C. The figure below (**Figure 22**) illustrates a failed polymerization attempt on the left and vertically printed fusilli structures on the right, demonstrating the optimized printing parameters.

Figure 22 - Fusilli printed **vertically** with '**3DP-F2**':
(*left*) lack of polymerization; (*right*) optimized parameters

Once the desired results were achieved by printing small-sized fusilli using the Asiga printer, the decision was made to exclusively continue with the '**3DP-F2**' resin, reverting to the use of the Elegoo Mars 3 MSLA printer, available at INAM, Universitat Jaume I. This was done to produce fusilli with a larger diameter and, most importantly, a longer length of up to 11.5 cm, which would allow for their subsequent use/insertion in the flow column. Naturally, transitioning to the other printer required re-optimizing the printing parameters. However, in this case, the process was much simpler as there were significantly fewer adjustable parameters. Following the previous approach, small-sized fusilli were initially printed in both horizontal and vertical orientations using the same parameters as the '**3DP-F1**' resin.

Remarkably, excellent print resolution was immediately achieved with these settings (**Figure 23**).

Figure 23 - Horizontally and vertically printed fusilli

Following that, to validate the improved resolution of the **3DP-F2** resin over the **3DP-F1** resin, the "Benchmark" structure was printed using both formulations (**Figure 24**). This direct comparison left no room for uncertainty regarding the choice of formulation to proceed with.

Figure 24 - Formulations' comparison: (*left*) **3DP-F1**; (*right*) **3DP-F2**

This second custom polymer formulation developed, '**3DP-F2**', demonstrated outstanding performance in terms of resolution in the Vat Photopolymerization process. The final printed objects exhibited exceptional detail and precision, surpassing the resolution achieved with previous materials. The optimized formulation successfully addressed the challenges associated with fine details and complex geometries. Subsequently, a wider range of fusilli types could be printed, particularly those measuring 11.5 cm in length with an approximate diameter of 1 cm. These fusilli were specifically designed to accommodate the insertion of four slender columns for subsequent application within the flow column. Moreover, a specific type of fusilli was successfully printed with a pitch of 1.8 mm, meaning that the characteristic distance between the solid layers was 0.9 mm, which in applications in reactor engineering can be formally considered a *microreactor* (**Figure 25c-d**). The final stage of the printing process, the complete structure, and select details are illustrated in **Figure 25**, for example in picture ***(d)*** it is possible to see ***each layer*** of the structure ***0.05 mm thickness***.

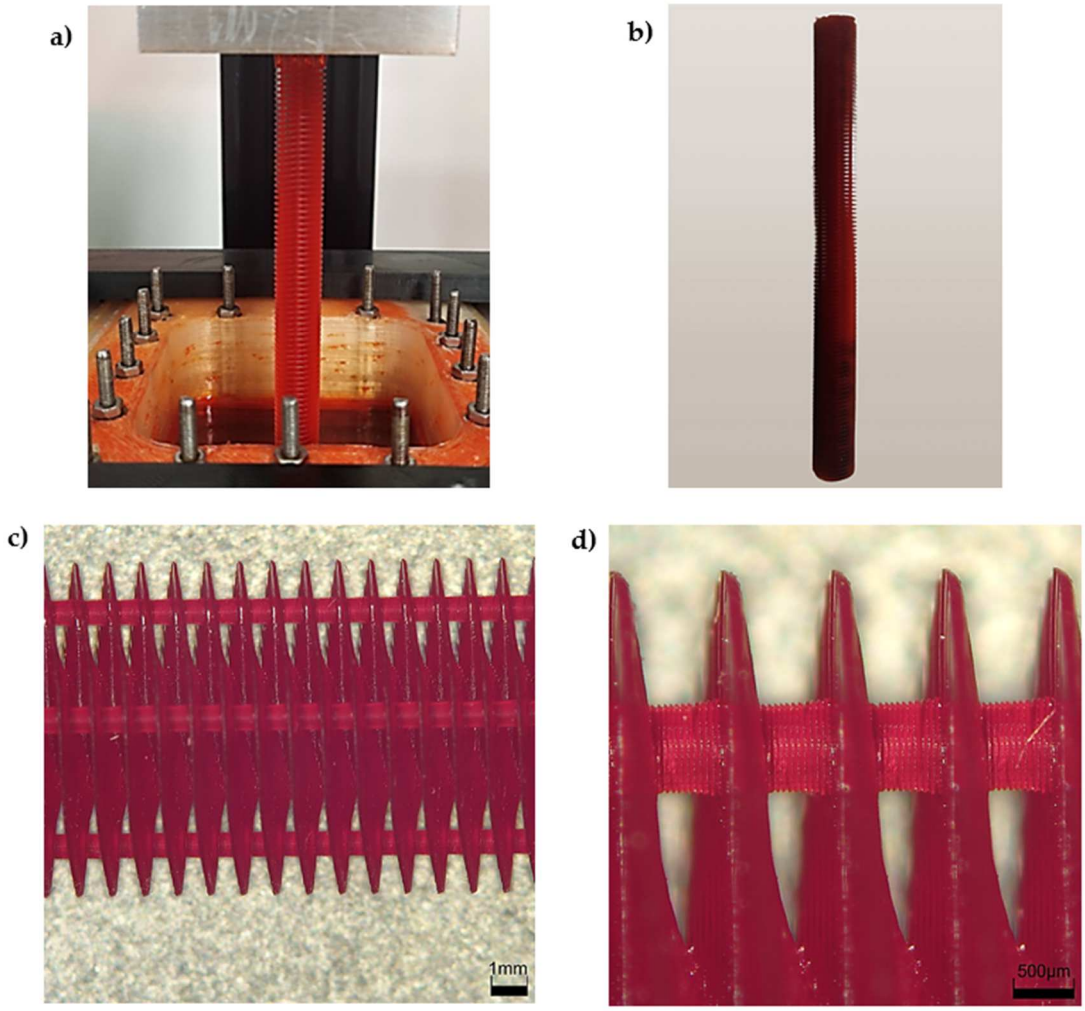

Figure 25 – **Structure R3-3DP-F2 [1.8 mm]**: ***(a)*** Printing process; ***(b)*** whole structure; ***(c)*** detail on the column; ***(d)*** detail on the layer resolution

As a final step, a resolution comparison was made between the 3DP-F2 resin and a commercial resin, "***3DP-COMM***" (Standard Translucent Photopolymer Resin, by Elegoo), which was used to print the R3 column as it required the highest possible resolution. The printing parameters of 3DP-COMM were obtained from the printer's website, where the various parameters for each type of commercial resin are listed for all Elegoo printers [57]. As shown in **Figure 26**, the resolution achieved with the 3DP-F2 formulation was not achievable even with ***3DP-COMM*** resin. The main problem with this resin was believed to be related to its viscosity and short printing times, which make it difficult for the resin to flow away from the structure in time before the subsequent layers were cured.

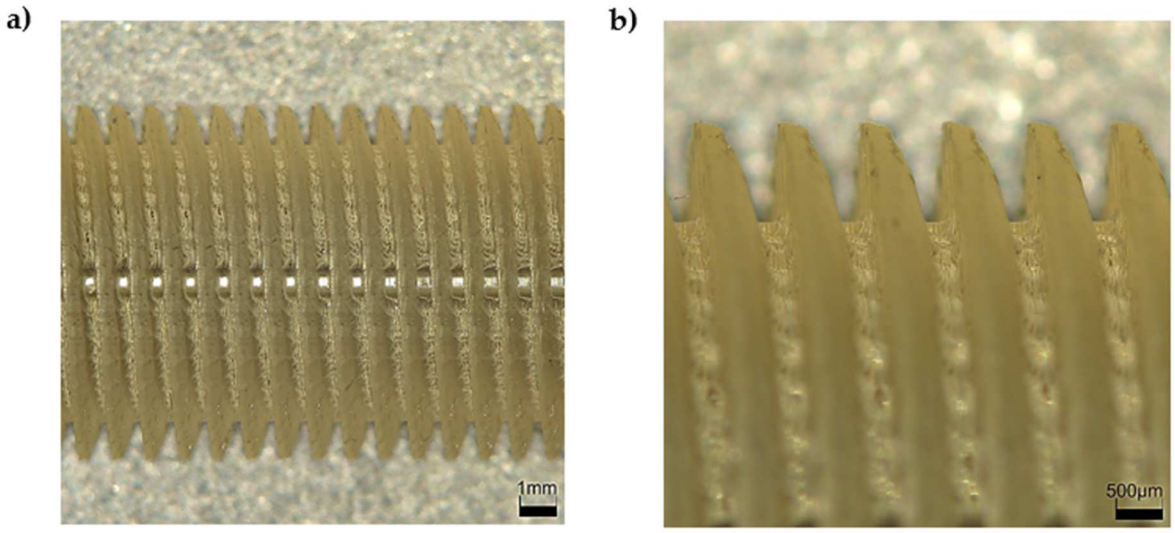

Figure 26 - **Structure R3-3DP-COMM [1.8 mm]**: ***(a)*** Detail on the column; ***(b)*** detail on the worse resolution

To conclude the development and optimisation of the formulations, below there is a summary table (**Table 1**) of the optimised parameters for each formulation in each printer used with different print orientations:

Table 1 - Optimised printing **parameters**

FORMULATION / PARAMETERS	**3DP-F1**	**3DP-F2**	**3DP-F2**	**3DP-F2**
Base Formulation	3DP-F1	PEGDA	PEGDA	3DP-F2
Printing orientation	Horizontal/Vertical	Horizontal	Vertical	Horizontal/Vertical
3D Printer	Elegoo Mars 3	Asiga MAX27UV	Asiga MAX27UV	Elegoo Mars 3
Layer thickness	0.05 mm	0.05 mm[a] (0.1 mm)[b]	0.05 mm[a] (0.1 mm)[b]	0.05 mm
Initial exposure time	22 s/layer	3.5 s/layer[b]	3.5 s/layer[b]	22 s/layer
Exposure time	18 s/layer	5 s/layer [a,c]	(5.45 ÷ 5.75) s/layer [a,d]	18 s/layer
Waiting time (after exposure)	2.5 s	0.5 s [a]	0.5 s [a]	2.5 s

[a] for **3DP-F2** layers; [b] for PEGDA layers; [c] with light intensity = 49 mW/cm^2; [d] starting from 5.75 s/layer lowering time with 0.1 s/layer every 40 layers until 5.45 s/layer (set until the end), light intensity = 40 mW/cm^2 and heater temperature = 30°C

3.2 - Characterization and Functionalization

3.2.1 3D Scanner

The use of the 3D scanner enabled the evaluation of print fidelity between the printed object and the CAD model. This involved creating a colorimetric map where the color green indicated no deviation between the CAD file and the printed object, while the colors red and blue represented positive and negative differences, respectively.

The accuracy of the printed structures was evaluated, starting with two structures (gyroid and fusilli-shaped ones) used to optimize the 3DP-F2 resin, that seemed to have a fairly good resolution. Their 3D scanned images are shown in **Figure 27**. It can be observed that the resolution of the gyroid was not optimal, which could potentially be attributed to an excessive amount of powder applied to make the structure visible to the 3D scanner. On the other hand, the other one exhibited better resolution, although some parts did not perfectly align with the CAD model. In both cases, the use of supports (dark red parts on the bottom) during printing was unavoidable.

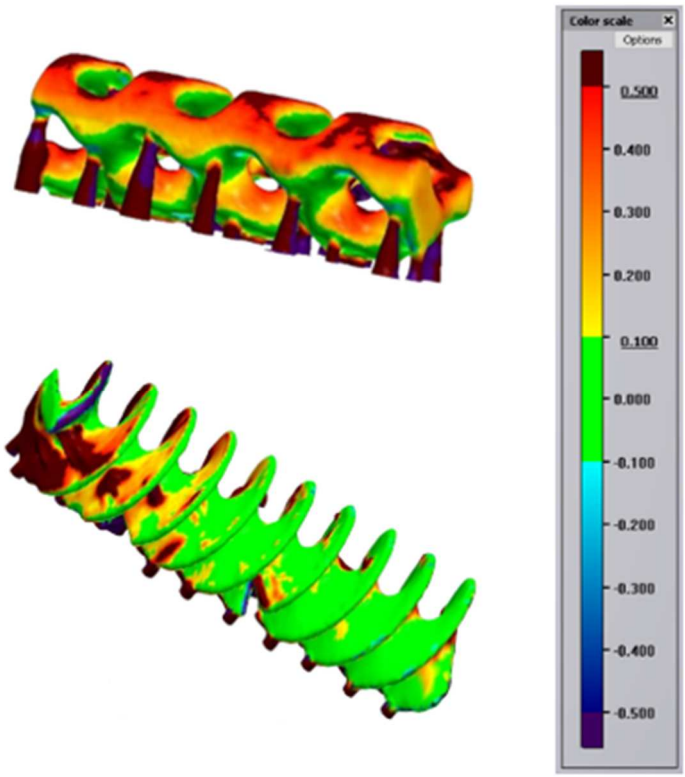

Figure 27 - 3D scan of gyroid and fusilli structure

A second evaluation was conducted on two vertically printed short fusilli. The first one (depicted above in ***3.1.2 Development*** in **Figure 17**) was created during the optimization of the ***3DP-F1*** resin before the additives were introduced. In contrast, the second one was printed using the ***3DP-F2*** formulation. As shown in **Figure 28**, it is evident that the second one exhibited better resolution, as the spiral structure is visible in finer detail.

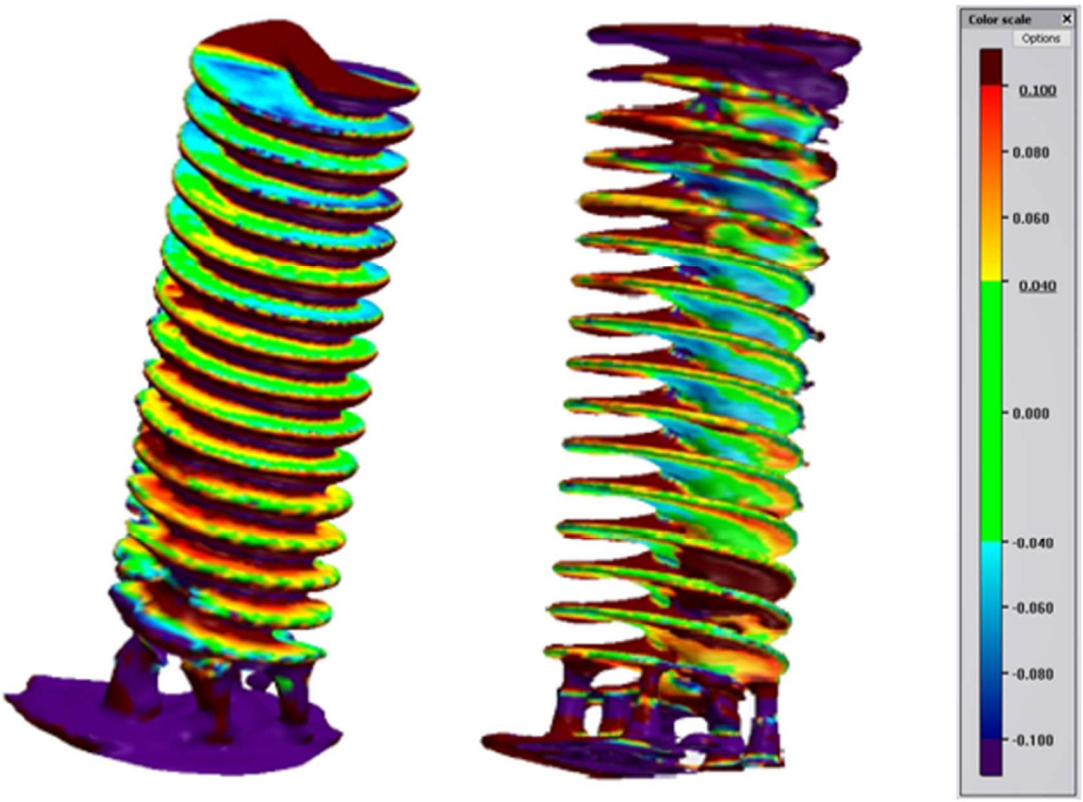

Figure 28 - 3D scan of 2.5 mm helix pitch fusilli: (***left***) while optimizing **3DP-F1**; (***right***) **3DP-F2**

The final assessment of print accuracy was performed on the **R3-3DP-F2** structure (previously shown with details up to each printing layer). As depicted in **Figure 29**, even with the 3D scanner the high quality of the print could be proved, due to the fact that the majority of the structure was coloured in green. However, it should be noted that this evaluation method does not provide extremely precise results, particularly for intricate structures where the distance between consecutive spirals is less than a millimetre (*0.9 mm*). In such cases, evaluating the interior of the structure becomes challenging, as it can be influenced by the presence of powder used to enhance visibility and by imperfect alignment between the scanned image and the CAD file, because achieving a perfect match between the scanned points and the CAD model is particularly difficult for highly detailed objects like these.

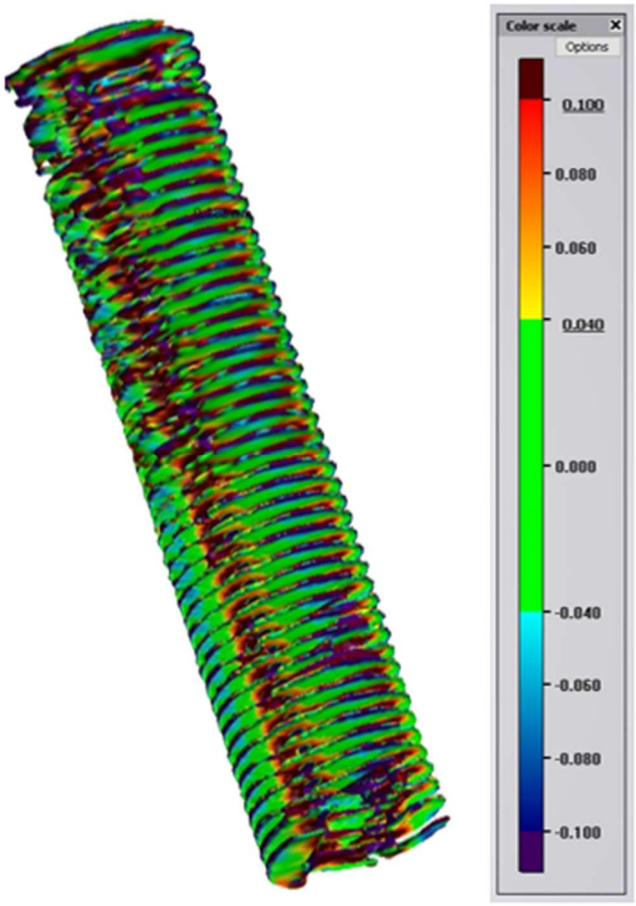

Figure 29 - 3D scan of structure **R3-3DP-F2**

3.2.2 Swelling Test

A swelling test was performed on vertically printed fusilli samples (**Figure 23**) to evaluate their weight and size changes when immersed in different solvents, aiming to determine the solvents that caused more or less pronounced alterations. The solvent used were selected thinking in a further utilization for the CO_2 cycloaddition reaction. The focus was primarily on swelling regarding the dimensions, particularly the diameter, in order to know the degree of reduction required from the original dimensions of the Solidworks-created object based on the solvent used. This degree of reduction aimed to facilitate the insertion of the 3D printed structure into the flow column (the results are shown in **Table 2**). This test, just related to the dimensions, was also made in the case of post-curing, with which a shrinkage of 0.5% was observed.

Table 2 – **Swelling test** in different solvents

Solvent	S_w% [a]	S_d% [a]
ACETONITRILE	2.2%	0.7%
ISOPROPANOL	0.0%	0.0%
WATER	2.2%	0.6%
80%/20% ACETONITRILE/WATER	5.0%	2.0%

([a]) **Sw**: Swelling by weight (1); **Sd** = Swelling by dimension (2)

In any case, based on these results, a decision was made to reduce the initial diameter of 1 cm for the various reactors R1, R2, and R3, as set in the CAD file, by **3%**. This reduction ensured the certainty that the reactor could be easily inserted into the column and, most importantly, that it would not break due to swelling in the event of solvent flow.

3.2.3 Functionalization

The functionalization was achieved through nucleophilic ring-opening of the epoxy ring, following the same method as described in the section '**2.5 – Functionalization**'. However, the conditions were varied to determine which ones yielded better functionalization results, initially evaluated qualitatively through transmission IR spectra and subsequently quantitatively through elemental analysis.
The use of different conditions allowed for comparisons based on the solvent reaction approach, timing of post-curing, reaction temperature, solvent type, and concentration. The quantities of hydrochloric acid and butyl imidazole remained constant throughout. The specific conditions are outlined in **Table 3**:

Table 3 - **Functionalization** conditions

Sample	Post-cured	Solvent	Temperature (°C)
1a	No	EtOH [a]	40
1b	No	EtOH [b]	40
2a	Yes	EtOH [b]	40
2b	Yes [c]	EtOH [b]	40
3	No	EtOH [b, d]	40
4a	No	DMF [b]	40
4b	No	DMF [b]	60
5	No	Acetonitrile/ H_2O (80%/20%) [b]	40

[a]Butyl Imidazole added later in drops; [b]Reagents added all together; [c]Post-curing made after functionalization; [d]EtOH volume reduced to a quarter of the initial one, resulting in higher concentration

3.2.3.1 FT-IR SPECTROSCOPY

Initially, the FTIR spectra of the key monomers (*GMA* and *PETA*) used to create the 3DP-F2 polymer resin, and of *Butyl imidazole*, the base reagent used for functionalization, were acquired (**Figure 30**) in order to understand better, thanks to the literature [58], which were the peaks that had to be taken into account when analysing the spectra related to the different conditions of functionalization.

In the spectrum of GMA and PETA, the following could be observed:

- The presence of the epoxy group (just in GMA), indicated by a band in the range of approximately 900-930 cm^{-1}
- The C=O stretching vibration of the ester group, appearing as a strong band around 1700-1750 cm^{-1}
- The C=C stretching vibrations of the acrylates group, exhibiting absorption bands around 1600-1650 cm^{-1}.

The subsequent features could be seen in the Butyl imidazole spectrum:

- The presence of the imidazole ring, characterized by a large absorption band in the range of 1500-1600 cm^{-1}
- The stretching vibrations of the C-H bonds in the butyl group, manifested as bands in the vicinity of 2850-2960 cm^{-1}.

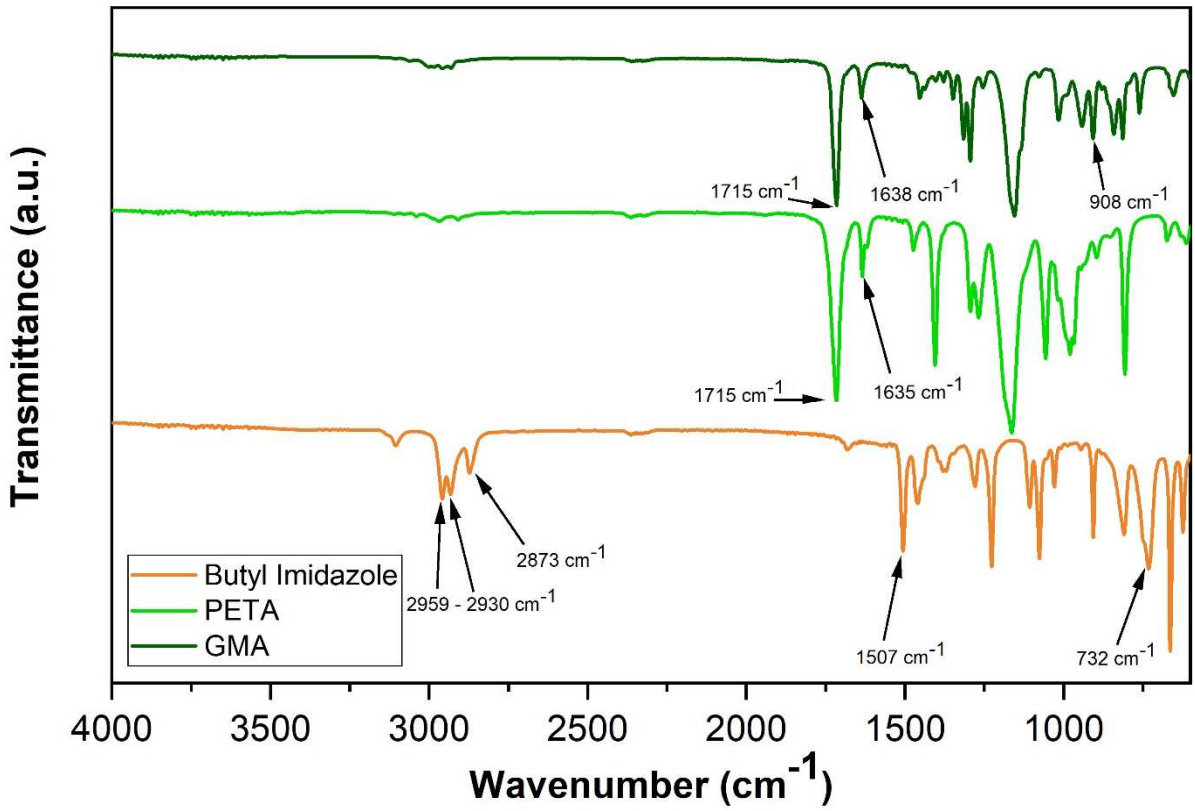

Figure 30 - FTIR spectra of **GMA**, **PETA**, and **Butyl Imidazole**

In the case of the samples that have been functionalized, it was possible to see some characteristic bands, related to the ***butyl imidazolium chloride*** **(ButImCl)**, which is an ionic liquid obtained after the functionalization, and based on the functional groups present in the molecule. *Butyl imidazolium chloride* contains several functional groups, including a butyl chain (C_4H_9), an imidazolium ring ($C_3H_3N_2$), and a chloride ion (Cl^-). Here below there are some of the bands that were observed in the FTIR spectra of the functionalized samples (examples are reported in **Figure 31** and in the Appendix):

- The butyl chain and methyl group exhibited characteristic absorption bands in the region of 2800-3000 cm^{-1}, corresponding to C-H stretching vibrations
- Since the imidazolium ring contains carbon-carbon double bonds, the C=C stretching vibrations could be typically seen in the range of 1500-1600 cm^{-1}.
- The chloride ion had an absorption band in the region of 700-800 cm^{-1}, corresponding to C-Cl stretching vibrations.

To assess the successful functionalization, the spectrum of the non-functionalized sample was compared with the spectra of the samples subjected to different conditions. It was evaluated whether, as reported in the literature [54], the ***appearance of imidazolium stretching bands*** at approximately *1560 cm^{-1}*, and in between *700 and 624 cm^{-1}* (highlighted in blue in the graphs), and the ***disappearance of epoxy stretching bands*** at around *905 cm^{-1}* (highlighted in red) could be observed.

The initial comparison between different conditions was based on the reaction approach, specifically whether to add Butyl imidazole dropwise after adding EtOH and HCl (**1a**), or to react everything together in batch (**1b**).

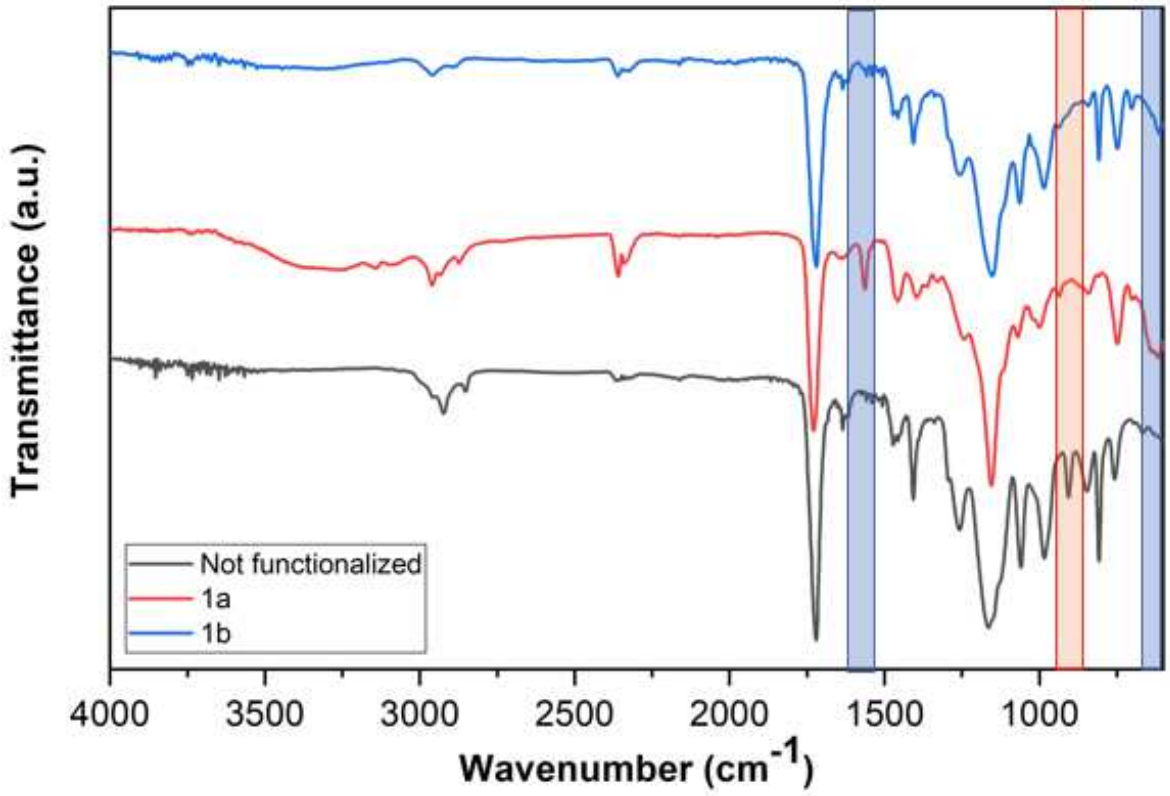

Figure 31 - Reaction approach comparison

From this comparison of spectra, it could be observed that the functionalization occurred correctly, particularly in the case where butyl imidazole was added subsequently (**1a**), because all the expected changes were observed. Instead, in the second case (**1b**), there was no appearance of the imidazolium stretching bands at 1560 cm^{-1}.

Furthermore, upon comparing these spectra with those of GMA and PETA, shown in **Figure 30**, it could be confirmed that polymerization took place because the C=C stretching bands of the acrylate group between 1600 and 1650 cm^{-1}, present in the spectra of the two monomers, decreased due to the formation of the polymer bond.

3.2.3.2 ELEMENTAL ANALYSIS

Using the results obtained from elemental analysis, a quantitative assessment of the functionalization was conducted. By knowing the mass, surface area of the sample, and the percentage of nitrogen present, it was possible to calculate the millimoles of butyl imidazole per gram of the disk and per square centimetre of surface area. The obtained results are presented in **Table 4**, where the average value for each condition was calculated based on multiple measurements.

Table 4 - Elemental Analysis results

Sample (*)	%N	%C	%H	mmol IL / g	mmol IL / cm^2
N.F.	/	56.895	4.355	/	/
1a	3.314	51.250	6.883	1.183	0.029
1b	0.981	52.995	6.339	0.350	0.008
2a	0.209	56.780	6.417	0.075	0.002
2b	0.946	53.680	6.357	0.338	0.008
3	0.745	55.180	6.418	0.266	0.006
4a	1.652	52.305	6.457	0.589	0.015
4b	4.968	48.025	7.338	1.773	0.049
5	0.798	53.215	6.340	0.285	0.007

(*) **N.F.** = Not Functionalized. With EtOH at 40°C: (**1a**) reaction in 2 steps; (**2a/2b**) post-curing before/after functionalization; (**3**) EtOH concentration reduced. With DMF: (**4a/4b**) at 40/60°C. With Acetonitrile and water: (**5**). [**Table 3**]

Knowing that the % of Nitrogen in **ButImCl** was approximately 17.44 and the molecular weight of **ButImCl** is 160.64 mg/mmol, the amount in mmol was calculated, allowing for a quantitative evaluation of the different conditions. From this table, it could be observed that higher amounts of mmol were obtained when the functionalization reaction took place in two steps, with the subsequent addition of butyl imidazole dropwise (**1a**), and when the temperature was raised to 60°C with DMF (**4b**). However, in the latter case, the resin transformed into a gel after functionalization, indicating that **ButImCl** remained predominantly on the surface.

This was confirmed by the IR spectrum, shown in Appendix in **Figure 42**, where the typical butyl imidazole bands are present in the region between 2800 and 3000 cm^{-1}.

Furthermore, it should be noted that this issue changes significantly depending on when post-curing was performed. If it was not performed (**1b**) or conducted after functionalization (**2b**), there was minimal difference, while if post-curing was carried out after printing the object (as commonly done with printed objects) but before functionalization (**2a**), the number of mmol decreased approximately by four times. Therefore, it is preferable either not to perform post-curing or to conduct it after functionalization.

3.2.4 – Thermogravimetric Analysis (TGA)

Another characterization method employed involved TGA analysis, in order to understand the thermal behaviour of 3D-printed objects (specifically, little disks) utilizing resin 3DP-F2 through a systematic investigation. The TGA graph for the functionalised and not functionalised discs is illustrated in **Figure 32**, showing the results obtained.

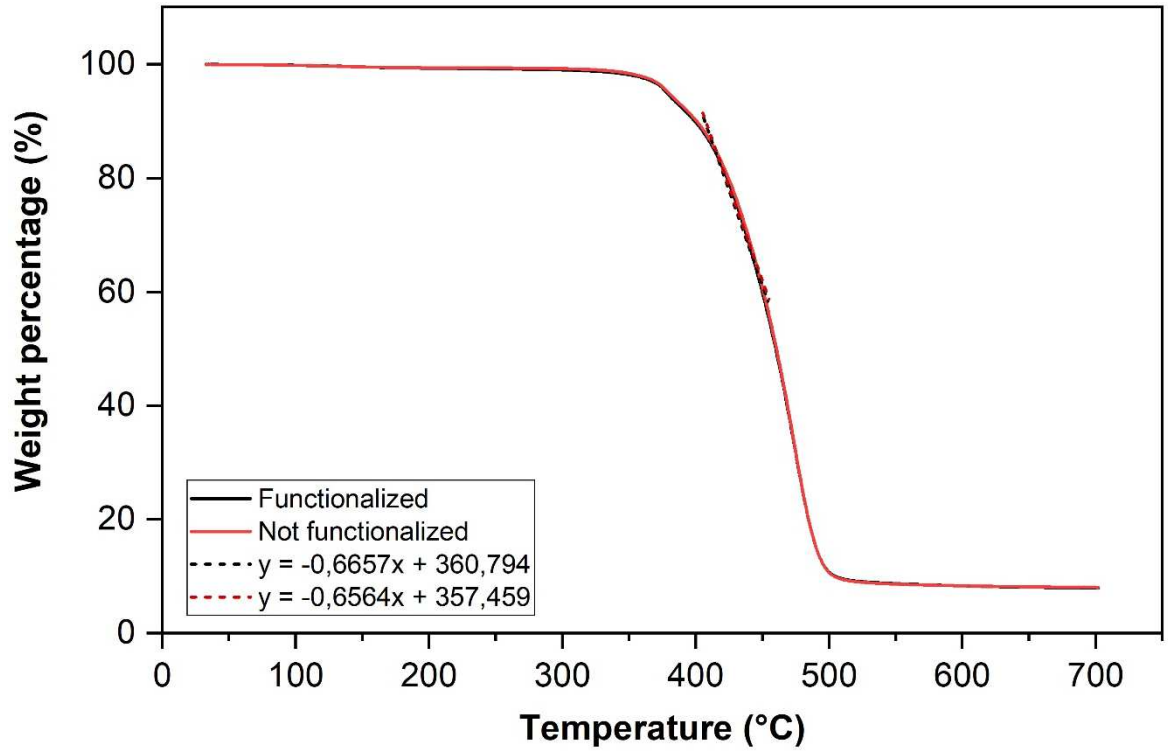

Figure 32 – **TGA** curve: Percent weight reduction as a function of temperature in functionalized and not functionalized samples

Subsequently, employing *Origin software*, the equations of tangent lines to the corresponding curves were determined, facilitating the calculation of the ***onset temperature*** by setting the y-value to 100%, and the 5% ***degradation temperature*** by setting y = 95%. The temperature values for both cases are listed in **Table 5**.

Table 5 – Temperatures obtained by **TGA** graph

	T degradation 5% (°C)	**T onset (°C)**
Functionalized	399.3	391.8
Not functionalized	399.8	392.2

Furthermore, heat flow was measured during TGA (as depicted in **Figure 33**); in this case this could be related to exothermic reactions occurring during thermal degradation. It could be noted that in the functionalized sample, a new peak appeared at 410°C, which could further indicate successful functionalization. Nevertheless, a conclusion could not be taken at this stage and more experiments should be carried out in this frame, for instance coupling FT-IR with TGA, and observing byproducts.

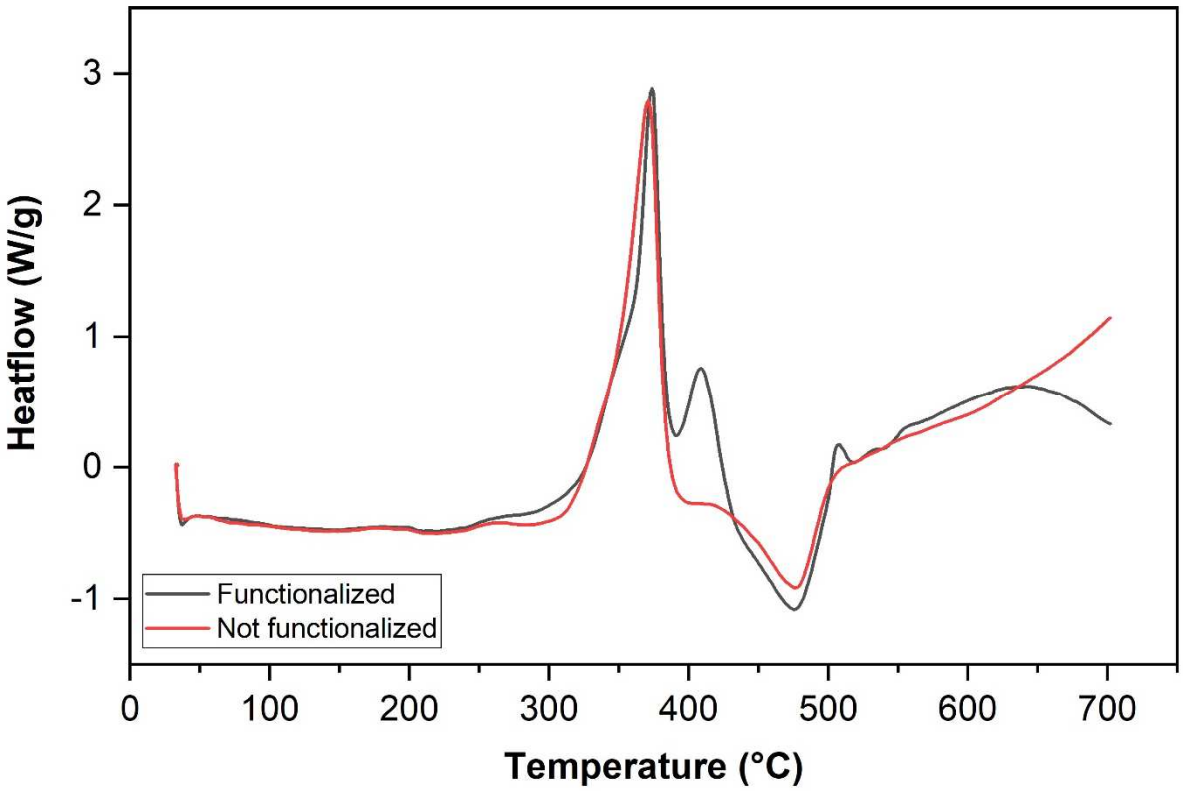

Figure 33 - Heat flow in function of temperature

3.2.5 - X-ray photoelectron spectroscopy (XPS)

Another characterization technique employed in this study was X-ray Photoelectron Spectroscopy (XPS), which was utilized to analyse two printed disc-shaped samples made from 3DP-F2 resin, one remaining not-functionalized (**Figure 34**) and the other subjected to functionalization (**Figure 35**), during the ongoing optimization of functionalization conditions. The objective was on assessing the increase in nitrogen percentage between the two cases.

By comparing the resulting graphs, it was observed that both samples exhibited the presence of certain elements, such as Si and Na, which should not have been detected. Furthermore, the not-functionalized sample showed the unexpected presence of nitrogen, which should have only appeared after the functionalization process. These undesired elements could potentially be attributed to resin contamination originating from the printing vat used. Nevertheless, it was found that the nitrogen percentage increased by only 0.1%, indicating that the employed functionalization method did not yield satisfactory results.

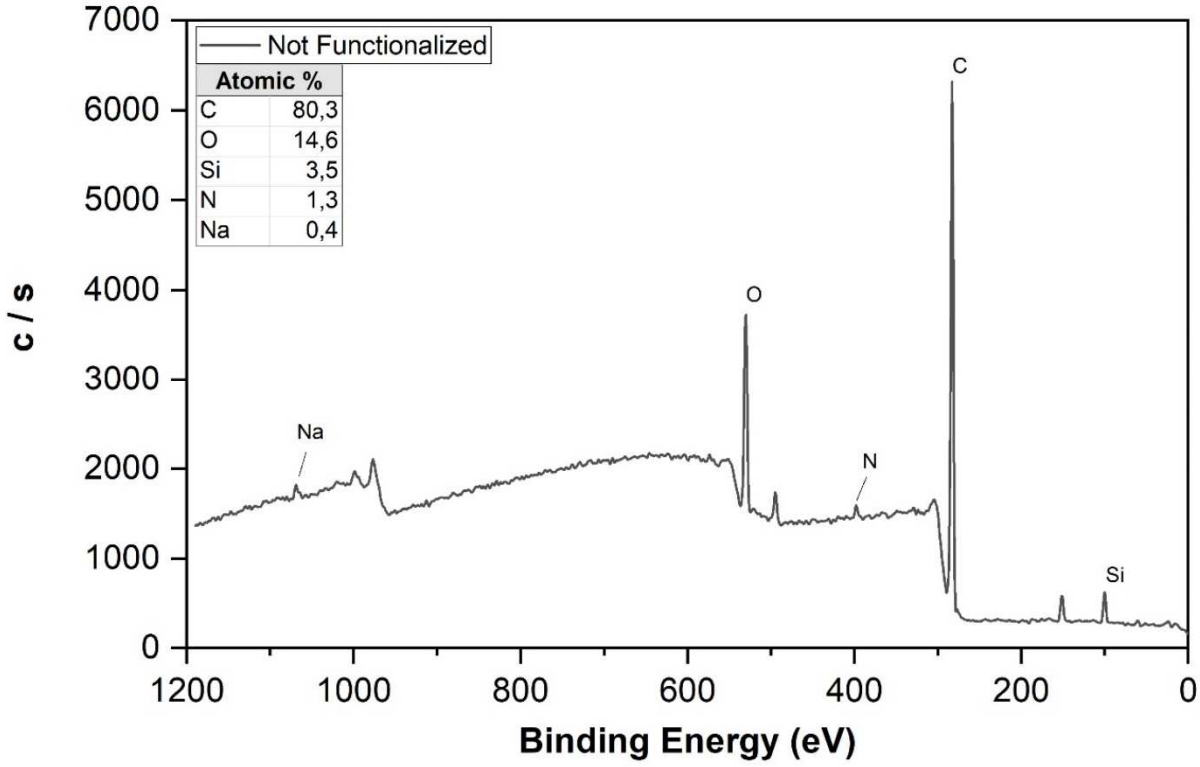

Figure 34 - **XPS** of not functionalized sample

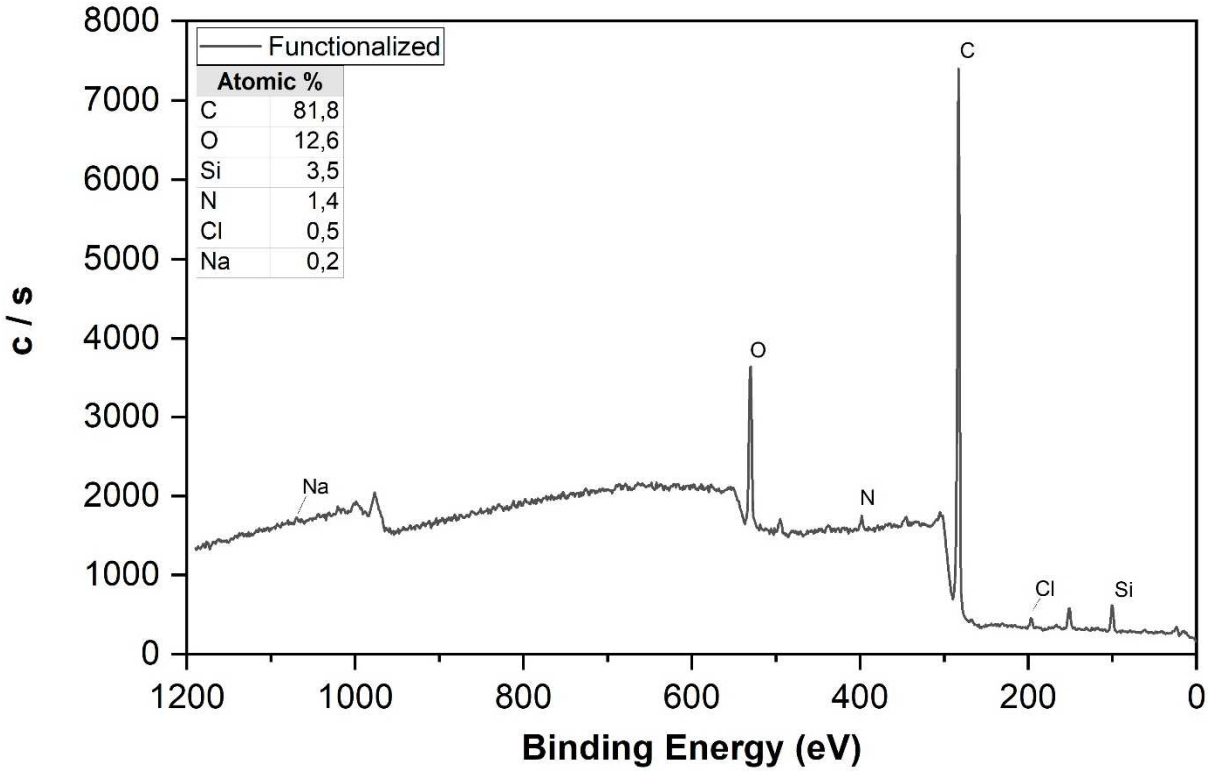

Figure 35 – **XPS** of functionalized sample

3.3 - CO_2 cycloaddition with 3DP reactor

The main application, for which the 3D printed reactors were created, was the cycloaddition reaction (**Figure 37a**), which parameters were optimized by employing a mixture consisting of ***styrene oxide*** and ***TBA.Br*** in Acetonitrile/H_2O (respectively 80% and 20% by volume). This solvent mixture was chosen as it was part of an integrated system developed within Dr. Sans research group at 'Universitat Jaume I', where the initial step was carried out electrochemically; anyway, this study solely focused on the evaluation of the subsequent stage. The impact of reactor structure variation was examined, revealing its significant influence on both selectivity (**Figure 37b**) and reproducibility of the reaction. Remarkably, the utilization of 3DP reactors yielded substantial improvements in both conversion and selectivity compared to the conventional packed bed reactor (***PBR***) comprised of polymeric beads of a commercial polymeric resin with a similar formulation to our 3DP polymers, as well as to a ***coiled tubular reactor*** (**Figure 36**).

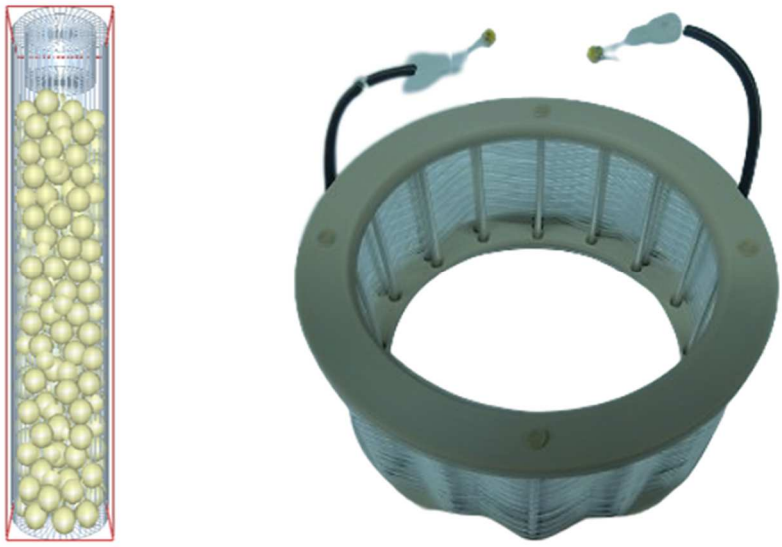

Figure 36 - (***Left***) Drawn example of PBR; (***Right***) Coiled tubular reactor of 5 mL volume

The 3DP reactors exhibited superior performance, achieving a conversion of 93±3% and a selectivity of 82±2% (**R1**), whereas the PBR and coil reactors demonstrated a conversion of 73±5% and 70±6% selectivity. Challenges related to pressure control and steady-state operation were encountered with the PBR and coil reactors. The coil reactor exhibited poor flow distribution, resulting in gas plugs maldistribution along the coil. This was evidenced by the difficulty in collecting product solution fractions with equal volumes at even time intervals, and the reproducibility of results was compromised, as indicated by the high error bars. In contrast, the utilization of 3DP structures improved fluid flow homogeneity, sample collection volume, and internal pressure within the column, leading to more stable process conditions and to increase productivity.

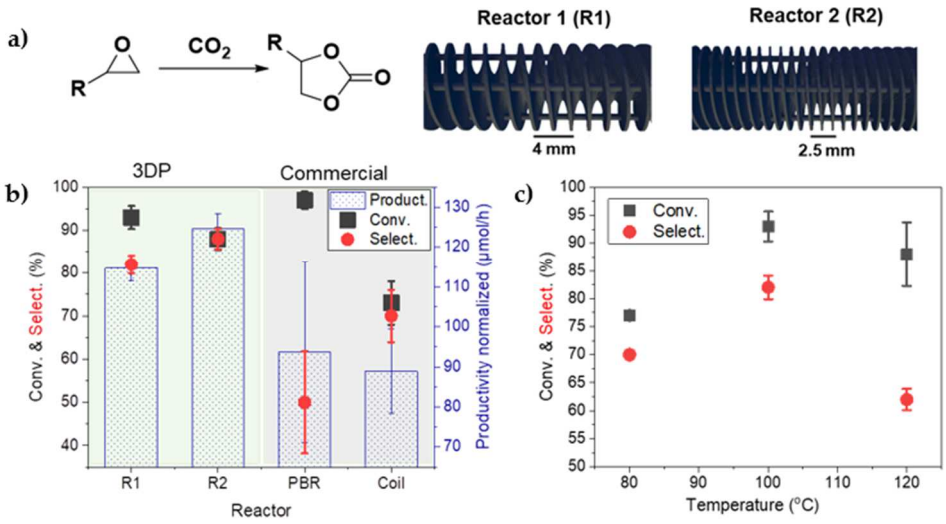

Figure 37 - **Optimization of CO_2 cycloaddition reaction in flow using styrene oxide.** (**a**) *SolidWorks design* of structured reactors. (**b**) *Evaluation of different flow reactors* (productivity adjusted according to residence time: R1 = 47 min; R2 = 51 min; PBR = 55 min; coil = 60 min). (**c**) *Temperature effect*.

The spiral configuration of the reactor, coupled with four internal columns, effectively enhanced the interface area between the liquid and gas phases, facilitating improved mass transfer, reactant-catalyst contact, and overall reaction rates. The presence of internal columns also enhanced the structural stability of the reactor. Although similar results were obtained from R1 and R2, R1 was selected for subsequent experiments due to its superior durability and extended potential usage. Furthermore, an increase in temperature to 120°C resulted in decreased selectivity, favouring the formation of byproducts (**Figure 37c**).

Using the ^{1}H NMR analysis (*e.g.*, **Figure 38**), it was possible to determine the mole quantities of the products and the unreacted species, which enabled the calculation of conversion and selectivity, using respectively equations (6) and (7).

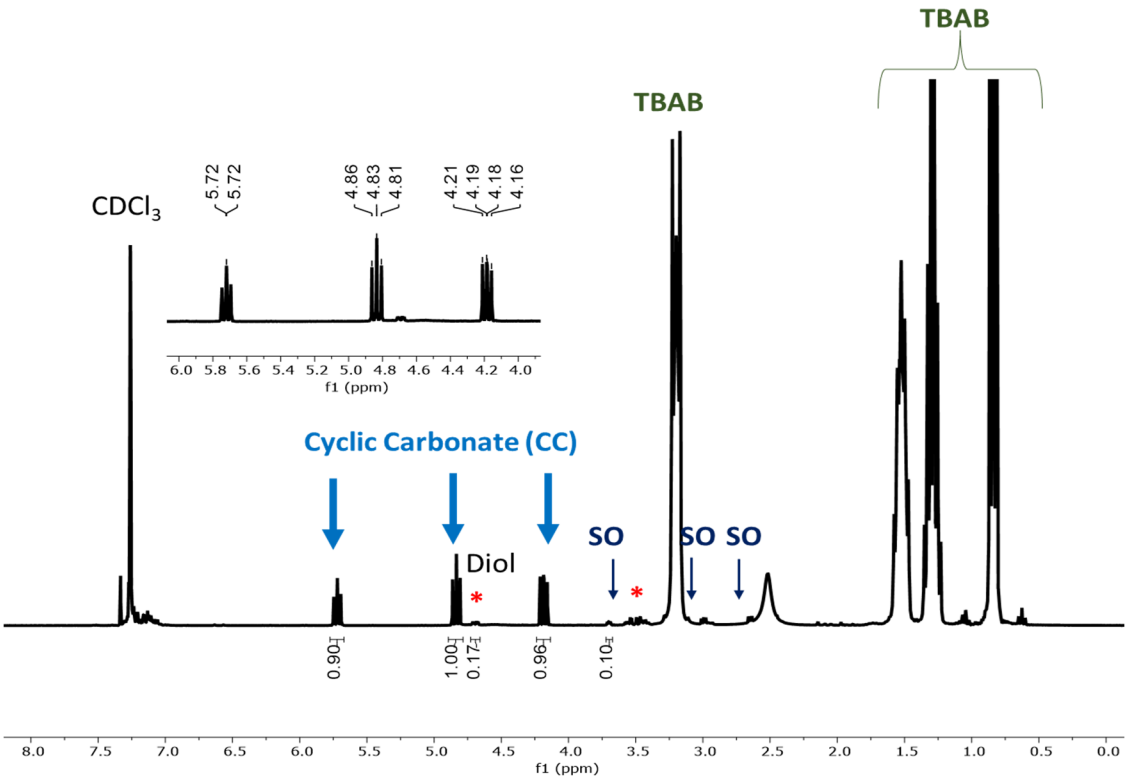

Figure 38 - **^{1}H NMR** (400 MHz, $CDCl_3$) of CO_2 cycloaddition using styrene oxide (SO) as substrate (optimized condition).

4. CONCLUSIONS

At the end of this thesis work, some interesting considerations can be made for the good results, such as the creation of 3D-printed catalytic reactors, which have been obtained after a great deal of research work, from which it is hoped future research work can continue in the direction taken.

Initially, the first objective of this research, which began at "***Politecnico di Torino***" and then continued at the *INAM* at "***Universitat Jaume I***" in Castellon de la Plana, Spain, was to optimise a polymer resin with a fairly high percentage of GMA, so as to have the greatest possible amount of epoxy groups, which were subsequently needed for the functionalisation reaction. As it turned out, the addition of additives, such as dye and the radical scavenger, to the base resin, thus obtaining **3DP-F2**, helped a great deal in improving the printing resolution, resulting in helical-shaped reactors with ever smaller pitches up to 1.8mm. Validating this excellent result was also the fact that with the commercial resin, **3DP-COMM**, supplied by the printer company itself, such a high level of resolution could not be achieved.

Once it was realised that the various reactors could now be printed without any problems, work began on characterising the resin and the objects themselves:

- The success of the print was evaluated using the *3D scanner*, thanks to which it was confirmed that the resolution of the print, even for the R3 reactor with a smaller pitch, was very good
- The *swelling* of the objects placed in different solvents was calculated to see where there was deformation and to know the exact size of the structure to fit the flow column according to the solvent used
- Different conditions were tried for functionalisation, which were evaluated first qualitatively using *FTIR spectroscopy* and then quantitatively using the results of *elemental analysis*, from which, knowing the % nitrogen present in the sample under the various conditions, it was judged that the best was the one carried out in two steps in which the sample was reacting (at a temperature of 40°C) with hydrochloric acid and ethanol and then with butyl imidazolium inserted in drops, because it contained the greatest amount of moles of the ionic liquid, ButImCl, obtained from the reaction
- Through the *TGA*, the degradation and onset temperatures of the functionalised and not-functionalised samples could be calculated respectively.

- Through XPS, while looking at the change of the nitrogen percentage in order to understand if the functionalization had properly worked, it was observed that in the vat there was probably some contamination.

The last step of this thesis was to try to put the 3D printed reactors in the flow column and run the cycloaddition reaction to transform CO_2 into cyclic carbonates. With the results given by *^1H NMR spectroscopy*, productivity, conversion and selectivity were calculated, obtaining higher and more reproducible values (smaller error bars) than two other commercial reactors. Subsequently, the **R2** reactor, which was found to be the best, was tested at different temperatures, obtaining the best results at a temperature of 100°C.

With this work, it was therefore possible to optimise a new polymer resin, which could be 3D printed with very high resolution and which could be functionalised, and thus achieve excellent conversion and selectivity results for the cycloaddition reaction, thus succeeding in transforming CO_2.
Obviously, there are still many steps to be taken to obtain even better results, with a higher level of functionalisation and consequently higher conversion and selectivity:

- improving the design of the reactors by forming a stronger structure, perhaps making the helix or the inner pillars thicker;
- improving the resin to achieve better reactions, changing the dye in order to have less colorant leakage or increasing the quantity of GMA to have more epoxy groups;
- working on the flow conditions in the system, introducing more CO_2;
- repeating XPS analysis to obtain more solid data on the functionalization method that was finally selected for this work or to improve its conditions;
- performing TGA with FT-IR and mass spectroscopy, to better elucidate degradation reaction;
- analysing the printed samples through SEM spectroscopy, which can help to observe surface modifications induced by functionalization reaction.

Appendix

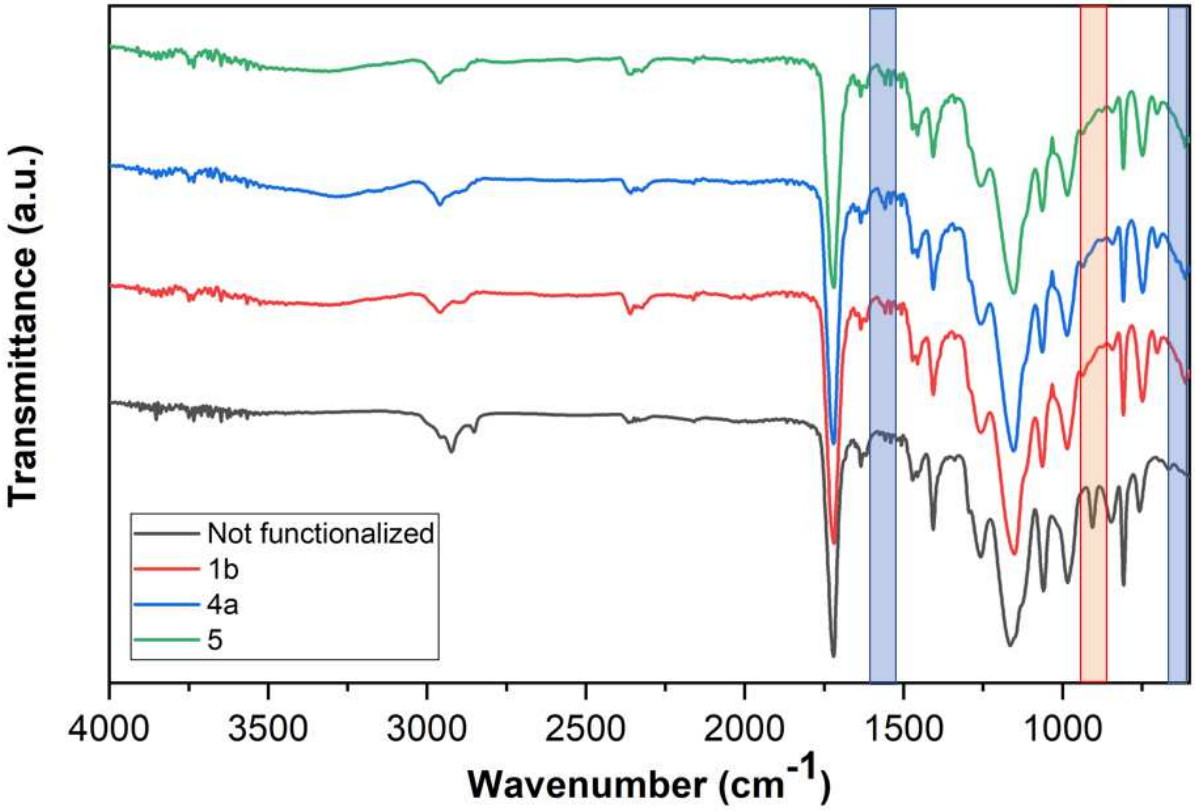

Figure 40 - Different solvents' comparison: (**1b**) EtOH; (**4a**) DMF; (**5**) Acetonitrile/Water (80/20)

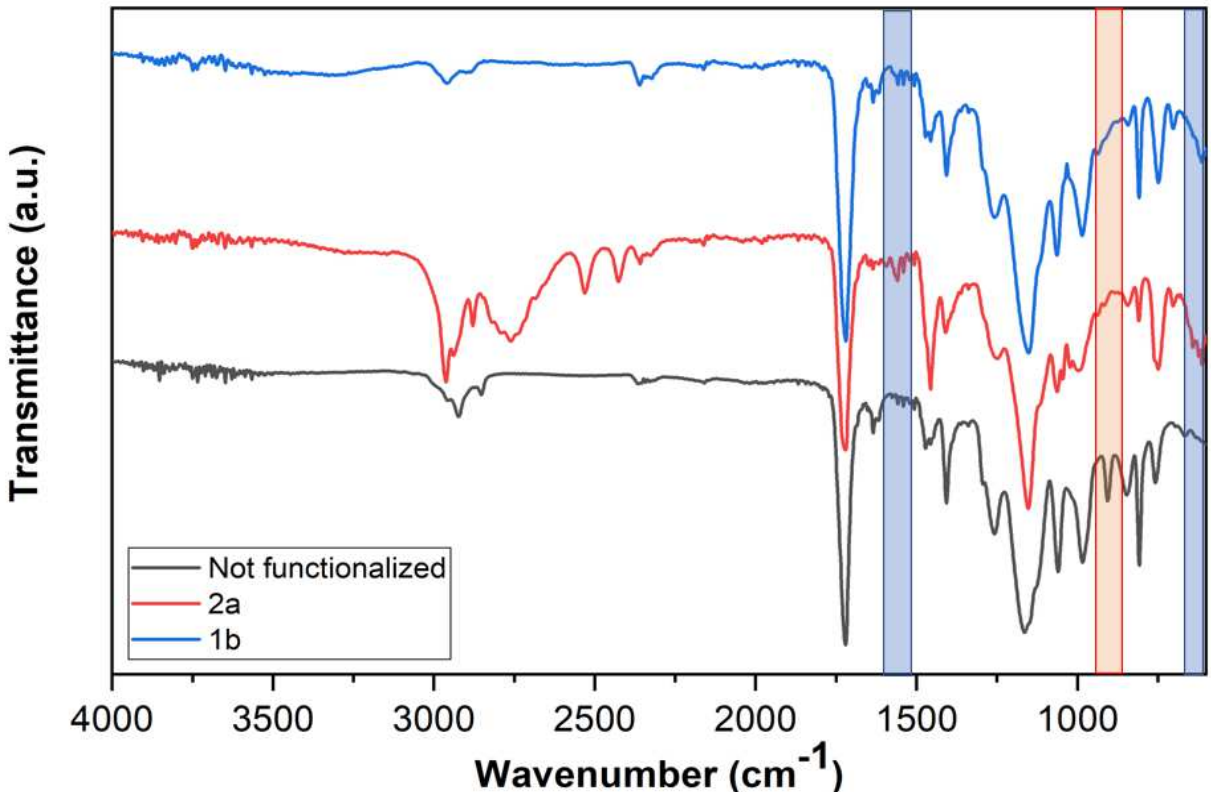

Figure 39 - (**1b**) Not post-cured; (**2a**) Post-cured.

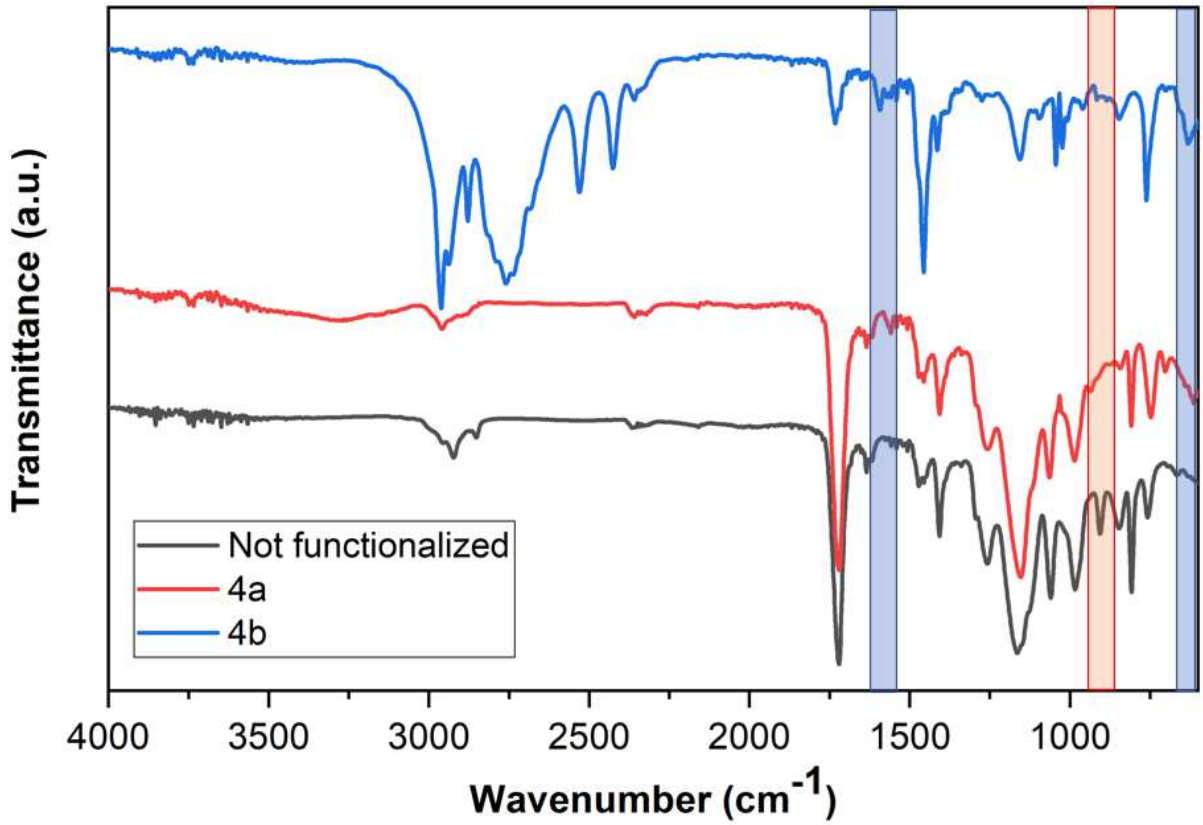

Figure 41 – Temperature comparison: (**4a**) 40°C; (**4b**) 60°C

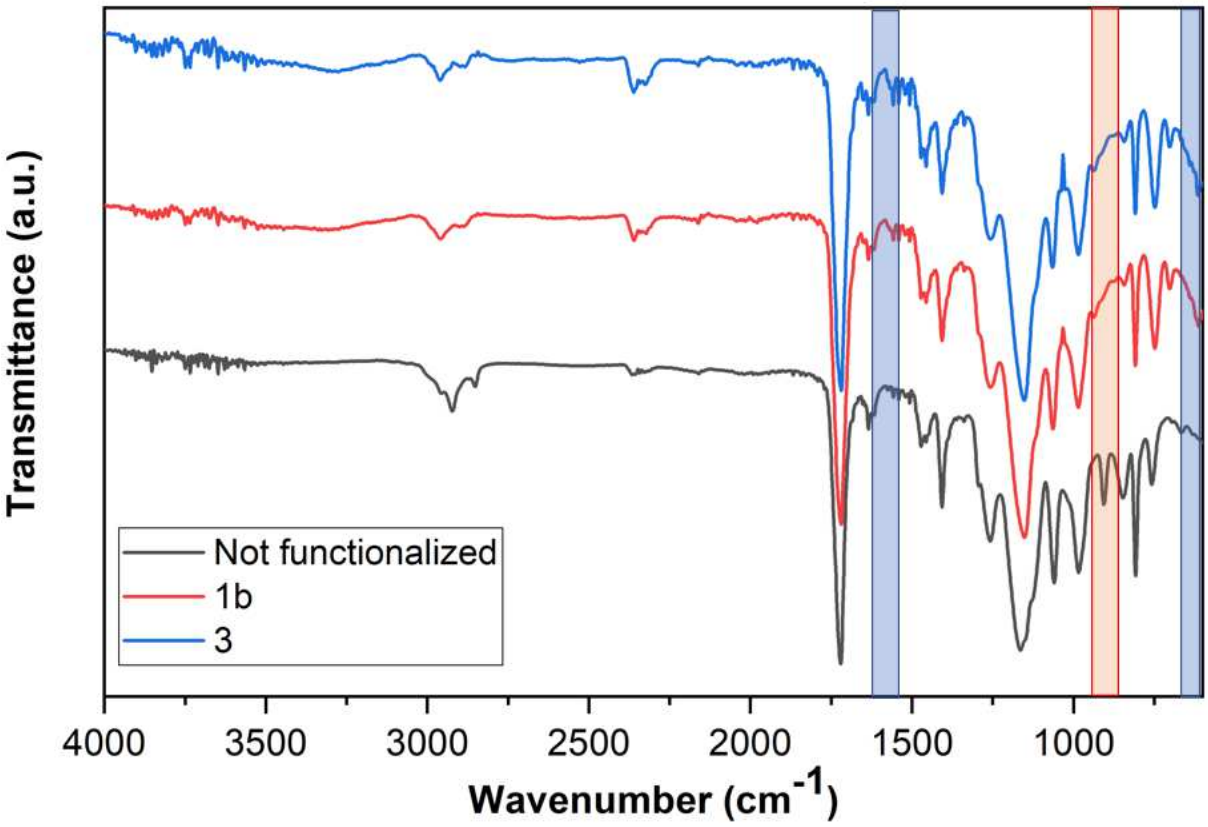

Figure 42 – Different solvent concentration: (**1b**) [EtOH]; (**3**) 1/4 [EtOH]

REFERENCES

[1] T. D. Ngo, A. Kashani, G. Imbalzano, K. T. Q. Nguyen, and D. Hui, 'Additive manufacturing (3D printing): A review of materials, methods, applications and challenges', *Composites Part B: Engineering*, vol. 143, pp. 172–196, Jun. 2018, doi: 10.1016/j.compositesb.2018.02.012.

[2] C. W. Hull and S. Gabriel, '(54) APPARATUS FOR PRODUCTION OF THREE-DIMENSONAL OBJECTS BY STEREOLITHOGRAPHY'.

[3] M. Pagac *et al.*, 'A Review of Vat Photopolymerization Technology: Materials, Applications, Challenges, and Future Trends of 3D Printing', *Polymers*, vol. 13, no. 4, Art. no. 4, Jan. 2021, doi: 10.3390/polym13040598.

[4] N. Shahrubudin, T. C. Lee, and R. Ramlan, 'An Overview on 3D Printing Technology: Technological, Materials, and Applications', *Procedia Manufacturing*, vol. 35, pp. 1286–1296, Jan. 2019, doi: 10.1016/j.promfg.2019.06.089.

[5] F. Zhang *et al.*, '3D printing technologies for electrochemical energy storage', *Nano Energy*, vol. 40, pp. 418–431, Oct. 2017, doi: 10.1016/j.nanoen.2017.08.037.

[6] Y. L. Tee, P. Tran, M. Leary, P. Pille, and M. Brandt, '3D Printing of polymer composites with material jetting: Mechanical and fractographic analysis', *Additive Manufacturing*, vol. 36, p. 101558, Dec. 2020, doi: 10.1016/j.addma.2020.101558.

[7] S. C. Ligon, R. Liska, J. Stampfl, M. Gurr, and R. Mülhaupt, 'Polymers for 3D Printing and Customized Additive Manufacturing', *Chem. Rev.*, vol. 117, no. 15, pp. 10212–10290, Aug. 2017, doi: 10.1021/acs.chemrev.7b00074.

[8] K. Rajaguru, T. Karthikeyan, and V. Vijayan, 'Additive manufacturing – State of art', *Materials Today: Proceedings*, vol. 21, pp. 628–633, Jan. 2020, doi: 10.1016/j.matpr.2019.06.728.

[9] H. Bikas, P. Stavropoulos, and G. Chryssolouris, 'Additive manufacturing methods and modelling approaches: a critical review', *Int J Adv Manuf Technol*, vol. 83, no. 1, pp. 389–405, Mar. 2016, doi: 10.1007/s00170-015-7576-2.

[10] L. Li, Q. Lin, M. Tang, A. J. E. Duncan, and C. Ke, 'Advanced Polymer Designs for Direct-Ink-Write 3D Printing', *Chemistry – A European Journal*, vol. 25, no. 46, pp. 10768–10781, 2019, doi: 10.1002/chem.201900975.

[11] C. A. Grande and T. Didriksen, 'Production of Customized Reactors by 3D Printing for Corrosive and Exothermic Reactions', *Ind. Eng. Chem. Res.*, vol. 60, no. 46, pp. 16720–16727, Nov. 2021, doi: 10.1021/acs.iecr.1c02791.

[12] M. C. Maier *et al.*, '3D Printed Reactors for Synthesis of Active Pharmaceutical Ingredients in Continuous Flow', *Org. Process Res. Dev.*, vol. 24, no. 10, pp. 2197–2207, Oct. 2020, doi: 10.1021/acs.oprd.0c00228.

[13] V. Sans, 'Emerging trends in flow chemistry enabled by 3D printing: Robust reactors, biocatalysis and electrochemistry', *Current Opinion in Green and Sustainable Chemistry*, vol. 25, p. 100367, Oct. 2020, doi: 10.1016/j.cogsc.2020.100367.

[14] P. Prabhakar *et al.*, '3D-Printed Microfluidics and Potential Biomedical Applications', *Frontiers in Nanotechnology*, vol. 3, 2021, Accessed: Jun. 08, 2023. [Online]. Available: https://www.frontiersin.org/articles/10.3389/fnano.2021.609355

[15] J. Zhu *et al.*, 'Recent advances in 3D printing for catalytic applications', *Chemical Engineering Journal*, vol. 433, p. 134341, Apr. 2022, doi: 10.1016/j.cej.2021.134341.

[16] J. W. Stansbury and M. J. Idacavage, '3D printing with polymers: Challenges among expanding options and opportunities', *Dental Materials*, vol. 32, no. 1, pp. 54–64, Jan. 2016, doi: 10.1016/j.dental.2015.09.018.
[17] S. Miralles-Comins, M. Zanatta, and V. Sans, 'Advanced Formulations Based on Poly(ionic liquid) Materials for Additive Manufacturing', *Polymers*, vol. 14, no. 23, Art. no. 23, Jan. 2022, doi: 10.3390/polym14235121.
[18] R. Brighenti, M. P. Cosma, L. Marsavina, A. Spagnoli, and M. Terzano, 'Multiphysics modelling of the mechanical properties in polymers obtained via photo-induced polymerization', *The International Journal of Advanced Manufacturing Technology*, vol. 117, Nov. 2021, doi: 10.1007/s00170-021-07273-2.
[19] Anandkumar R. Kannurpatti, Robert W. Peiffer, C. Allan Guymon, and Christopher N. Bowman, 'Photochemistry of polymers: photopolymerization fundamentals and applications', presented at the Proc.SPIE, Aug. 1996, p. 1028508. doi: 10.1117/12.245263.
[20] A. B. Scranton, C. N. Bowman, R. W. Peiffer, American Chemical Society, and American Chemical Society, Eds., *Photopolymerization: fundamentals and applications*. in ACS symposium series, no. 673. Washington, DC: American Chemical Society, 1997.
[21] J.-P. Pascault and R. J. J. Williams, 'Thermosetting Polymers', in *Handbook of Polymer Synthesis, Characterization, and Processing*, E. Saldívar-Guerra and E. Vivaldo-Lima, Eds., Hoboken, NJ, USA: John Wiley & Sons, Inc., 2013, pp. 519–533. doi: 10.1002/9781118480793.ch28.
[22] R. J. Mondschein, A. Kanitkar, C. B. Williams, S. S. Verbridge, and T. E. Long, 'Polymer structure-property requirements for stereolithographic 3D printing of soft tissue engineering scaffolds', *Biomaterials*, vol. 140, pp. 170–188, Sep. 2017, doi: 10.1016/j.biomaterials.2017.06.005.
[23] F. P. W. Melchels, J. Feijen, and D. W. Grijpma, 'A review on stereolithography and its applications in biomedical engineering', *Biomaterials*, vol. 31, no. 24, pp. 6121–6130, Aug. 2010, doi: 10.1016/j.biomaterials.2010.04.050.
[24] M. Vaezi, H. Seitz, and S. Yang, 'A review on 3D micro-additive manufacturing technologies', *The International Journal of Advanced Manufacturing Technology*, vol. 67, Jul. 2012, doi: 10.1007/s00170-012-4605-2.
[25] M. Podgórski, S. Huang, and C. N. Bowman, 'Additive Manufacture of Dynamic Thiol–ene Networks Incorporating Anhydride-Derived Reversible Thioester Links', *ACS Appl. Mater. Interfaces*, vol. 13, no. 11, pp. 12789–12796, Mar. 2021, doi: 10.1021/acsami.0c18979.
[26] A. Bagheri and J. Jin, 'Photopolymerization in 3D Printing', *ACS Appl. Polym. Mater.*, vol. 1, no. 4, pp. 593–611, Apr. 2019, doi: 10.1021/acsapm.8b00165.
[27] P. Fiedor and J. Ortyl, 'A New Approach to Micromachining: High-Precision and Innovative Additive Manufacturing Solutions Based on Photopolymerization Technology', *Materials*, vol. 13, no. 13, Art. no. 13, Jan. 2020, doi: 10.3390/ma13132951.
[28] S.-G. You, S.-M. You, S.-Y. Kang, S.-Y. Bae, and J.-H. Kim, 'Evaluation of the adaptation of complete denture metal bases fabricated with dental CAD-CAM systems: An in vitro study', *The Journal of Prosthetic Dentistry*, vol. 125, no. 3, pp. 479–485, Mar. 2021, doi: 10.1016/j.prosdent.2020.01.039.
[29] C. Yu *et al.*, 'Photopolymerizable Biomaterials and Light-Based 3D Printing Strategies for Biomedical Applications', *Chem Rev*, vol. 120, no. 19, pp. 10695–10743, Oct. 2020, doi: 10.1021/acs.chemrev.9b00810.
[30] S. J. Rowan, '100th Anniversary of Macromolecular Science Viewpoints', *ACS Macro Lett.*, vol. 10, no. 4, pp. 466–468, Apr. 2021, doi: 10.1021/acsmacrolett.1c00175.

[31] E. Andrzejewska, 'Photopolymerization kinetics of multifunctional monomers', *Progress in Polymer Science*, vol. 26, no. 4, pp. 605–665, May 2001, doi: 10.1016/S0079-6700(01)00004-1.
[32] Y. Yagci, S. Jockusch, and N. J. Turro, 'Photoinitiated Polymerization: Advances, Challenges, and Opportunities', *Macromolecules*, vol. 43, no. 15, pp. 6245–6260, Aug. 2010, doi: 10.1021/ma1007545.
[33] R. Schwalm, 'Photoinitiators and Photopolymerization', in *Encyclopedia of Materials: Science and Technology*, K. H. J. Buschow, R. W. Cahn, M. C. Flemings, B. Ilschner, E. J. Kramer, S. Mahajan, and P. Veyssière, Eds., Oxford: Elsevier, 2001, pp. 6946–6951. doi: 10.1016/B0-08-043152-6/01230-4.
[34] M. Cziferszky, C. Turecek, B. Kaiser, J. Stampfl, R. Liska, and F. Varga, 'Evaluation of Biocompatible Photopolymers I: Photoreactivity and Mechanical Properties of Reactive Diluents', *Journal of Macromolecular Science Part a-Pure and Applied Chemistry*, vol. 44, pp. 547–557, Mar. 2007, doi: 10.1080/10601320701235958.
[35] I. Roppolo *et al.*, '3D printable light-responsive polymers', *Mater. Horiz.*, vol. 4, no. 3, pp. 396–401, May 2017, doi: 10.1039/C7MH00072C.
[36] S. Zeng *et al.*, 'Ionic-Liquid-Based CO2 Capture Systems: Structure, Interaction and Process', *Chem. Rev.*, vol. 117, no. 14, pp. 9625–9673, Jul. 2017, doi: 10.1021/acs.chemrev.7b00072.
[37] H. Nulwala, A. Mirjafari, and X. Zhou, 'Ionic liquids and poly(ionic liquid)s for 3D printing – A focused mini-review', *European Polymer Journal*, vol. 108, pp. 390–398, Nov. 2018, doi: 10.1016/j.eurpolymj.2018.09.023.
[38] A. Eftekhari and T. Saito, 'Synthesis and properties of polymerized ionic liquids', *European Polymer Journal*, vol. 90, pp. 245–272, May 2017, doi: 10.1016/j.eurpolymj.2017.03.033.
[39] J. Podder, B. R. Patra, F. Pattnaik, S. Nanda, and A. K. Dalai, 'A Review of Carbon Capture and Valorization Technologies', *Energies*, vol. 16, no. 6, Art. no. 6, Jan. 2023, doi: 10.3390/en16062589.
[40] C. B. Peres, P. M. R. Resende, L. J. R. Nunes, and L. C. de Morais, 'Advances in Carbon Capture and Use (CCU) Technologies: A Comprehensive Review and CO2 Mitigation Potential Analysis', *Clean Technologies*, vol. 4, no. 4, Art. no. 4, Dec. 2022, doi: 10.3390/cleantechnol4040073.
[41] L. Guo, K. J. Lamb, and M. North, 'Recent developments in organocatalysed transformations of epoxides and carbon dioxide into cyclic carbonates', *Green Chem.*, vol. 23, no. 1, pp. 77–118, Jan. 2021, doi: 10.1039/D0GC03465G.
[42] A. Rehman, F. Saleem, F. Javed, A. Ikhlaq, S. W. Ahmad, and A. Harvey, 'Recent advances in the synthesis of cyclic carbonates via CO2 cycloaddition to epoxides', *Journal of Environmental Chemical Engineering*, vol. 9, no. 2, p. 105113, Apr. 2021, doi: 10.1016/j.jece.2021.105113.
[43] A. Soliman, N. AlAmoodi, G. N. Karanikolos, C. C. Doumanidis, and K. Polychronopoulou, 'A Review on New 3-D Printed Materials' Geometries for Catalysis and Adsorption: Paradigms from Reforming Reactions and CO2 Capture', *Nanomaterials*, vol. 10, no. 11, Art. no. 11, Nov. 2020, doi: 10.3390/nano10112198.
[44] J. Peng and Y. Deng, 'Cycloaddition of carbon dioxide to propylene oxide catalyzed by ionic liquids', *New J. Chem.*, vol. 25, no. 4, pp. 639–641, Jan. 2001, doi: 10.1039/B008923K.

[45] A. A. Chaugule, A. H. Tamboli, and H. Kim, 'Ionic liquid as a catalyst for utilization of carbon dioxide to production of linear and cyclic carbonate', *Fuel*, vol. 200, pp. 316–332, Jul. 2017, doi: 10.1016/j.fuel.2017.03.077.
[46] V. Caló, A. Nacci, A. Monopoli, and A. Fanizzi, 'Cyclic Carbonate Formation from Carbon Dioxide and Oxiranes in Tetrabutylammonium Halides as Solvents and Catalysts', *Org. Lett.*, vol. 4, no. 15, pp. 2561–2563, Jul. 2002, doi: 10.1021/ol026189w.
[47] J. Sun, S. Zhang, W. Cheng, and J. Ren, 'Hydroxyl-functionalized ionic liquid: a novel efficient catalyst for chemical fixation of CO2 to cyclic carbonate', *Tetrahedron Letters*, vol. 49, no. 22, pp. 3588–3591, May 2008, doi: 10.1016/j.tetlet.2008.04.022.
[48] B. Wang *et al.*, 'One-pot reaction of CO2, epichlorohydrin and amine to synthesize 4-(phenylamino)methyl-ethylene carbonate catalyzed by ionic liquids', *Journal of CO2 Utilization*, vol. 1, pp. 88–91, Jun. 2013, doi: 10.1016/j.jcou.2013.02.001.
[49] 'Merck | Spain | Life Science Products & Service Solutions'. https://www.sigmaaldrich.com/ES/en (accessed May 31, 2023).
[50] 'ELEGOO Mars 3 ULTRA 4K Mono LCD 3D Printer', *ELEGOO Official*. https://www.elegoo.com/en-es/products/elegoo-mars-3-lcd-3d-printer (accessed May 30, 2023).
[51] 'Max – Asiga'. https://www.asiga.com/max/ (accessed May 30, 2023).
[52] D. A. Shirley, 'High-Resolution X-Ray Photoemission Spectrum of the Valence Bands of Gold', *Phys. Rev. B*, vol. 5, no. 12, pp. 4709–4714, Jun. 1972, doi: 10.1103/PhysRevB.5.4709.
[53] A. Akelah and D. C. Sherrington, 'Application of functionalized polymers in organic synthesis', *Chem. Rev.*, vol. 81, no. 6, pp. 557–587, Dec. 1981, doi: 10.1021/cr00046a003.
[54] D. Valverde *et al.*, 'Towards highly efficient continuous-flow catalytic carbon dioxide cycloadditions with additively manufactured reactors', *Green Chem.*, vol. 24, no. 8, pp. 3300–3308, 2022, doi: 10.1039/D1GC04593H.
[55] '1-Butylimidazole 4316-42-1 | TCI AMERICA'. https://www.tcichemicals.com/US/en/p/B2345 (accessed Jun. 16, 2023).
[56] 'Essentials of Chemical Reaction Engineering, Scott Fogler, 9780134663890 .
[57] 'ELEGOO resin settings on Mars Series & Saturn Series & Jupiter(official) - 20230414.xlsx', *Google Docs*. https://drive.google.com/file/d/1_jnyMfNkm4sPJhKyN46ey5CO-ks4MRyR/view?usp=sharing&usp=embed_facebook (accessed Jun. 23, 2023).
[58] A. B. D. Nandiyanto, R. Oktiani, and R. Ragadhita, 'How to Read and Interpret FTIR Spectroscope of Organic Material', *Indonesian Journal of Science and Technology*, vol. 4, no. 1, Art. no. 1, Mar. 2019, doi: 10.17509/ijost.v4i1.15806.

RINGRAZIAMENTI

Giunto al termine di questo percorso di studi, posso solo essere soddisfatto dell'obiettivo raggiunto: non è stato semplice, ci sono stati tanti momenti di sconforto quando le cose non andavano come sperato, ma con grande forza di volontà sono arrivato a compiere il mio obiettivo.

Un doveroso ringraziamento va al Dott. Ignazio Roppolo, che, come relatore di tesi, mi ha sempre seguito attentamente nei progressi fatti a Torino e anche successivamente a Castellon, chiedendo aggiornamenti e dandomi preziosi consigli sia per il lavoro in laboratorio sia per il lavoro di stesura della tesi.

Sono, inoltre, molto riconoscente al Dott. Victor Sans e alla Dott.ssa Marcileia Zanatta, i quali mi hanno accolto con calore alla "Universitat Jaume I" di Castellon fin da subito, molto contenti per iniziare un progetto in collaborazione con il Politecnico di Torino, e mi hanno seguito da vicino per tutto il tempo della mia permanenza in Spagna e non solo, prendendo parte anche alle ultime correzioni per questo lavoro.

Sono molto grato ai dottorandi incontrati sia a Torino sia a Castellon per essere stati sempre molto gentili con me e pronti ad aiutarmi, soprattutto quando avevo bisogno di consigli pratici per affrontare i momenti in cui i risultati non erano quelli sperati.

Un ringraziamento molto speciale va ai miei genitori, ai miei fratelli e ai miei nonni per avermi supportato sempre in qualsiasi situazione e aver creduto in me dall'inizio alla fine spingendomi con il loro affetto ad arrivare a questo traguardo.

In questi lunghi anni di studi al Politecnico, ho avuto modo di consolidare rapporti di amicizia già instaurati in passato, con i miei amici di Pont, Martina, Mattia e Valentina, con cui ci conosciamo da quando eravamo bambini, con i miei amici del liceo, Alessia, Eugenio, Filippo, Francesco, Irene, Gianluca, Giosuè e Salvatore, con cui per ovvi motivi ci vediamo di meno, ma quando ci incontriamo sono sempre bei momenti, con i miei amici Daniele e Giovanni, con cui abbiamo condiviso totalmente il percorso universitario, e con Mattia, che è stato mio coinquilino per 6 anni, con cui abbiamo vissuto moltissime sessioni d'esame.

In più, grazie alle esperienze vissute all'estero, ho potuto conoscere moltissime persone, tra cui gli amici dell'Erasmus a Karlsruhe, Clara, Cristina, Elena, Lucas, Maxime, Hugo, Deniz, Perrine, Pietro e Susanna (a cui va un grazie particolare per aver condiviso la maggior parte della vita universitaria, una volta tornati dalla

Germania), con i quali siamo riusciti a creare un rapporto così bello, per cui anche se tutti siamo in luoghi diversi e lontani riusciamo comunque a incontrarci di tanto in tanto in giro per l'Europa, e gli amici di questi ultimi 4 mesi trascorsi a Castellon per svolgere il lavoro di tesi, Andrea, Francesco e Ylenia, che mi hanno supportato sempre e con cui abbiamo vissuto parecchi e indimenticabili momenti di divertimento in territorio spagnolo.